FREQUENCY RESPONSE OF A SUPPORTED THERMOCOUPLE WIRE: EFFECTS OF AXIAL CONDUCTION

LEWIS GRANT
IN-35-CR
7614
P-57

Progress Report
October 1990 - March 1991

L. J. Forney
School of Chemical Engineering
Georgia Institute of Technology
Atlanta, Georgia 30332

E. L. Meeks
Microelectronics Research Center
Georgia Institute of Technology
Atlanta, Georgia 30332

G. C. Fralick
Research Sensor Technology Branch
NASA - Lewis Research Center
Cleveland, Ohio 44135

Georgia Institute of Technology
April, 1991
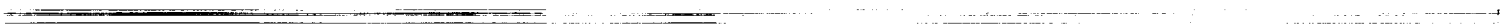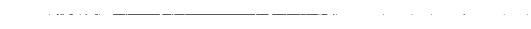
Frequency Response of a Supported Thermocouple Wire :

Effects of Axial Conduction

L. J. Forney
School of Chemical Engineering
Georgia Institute of Technology
Atlanta, Georgia 30332

E. L. Meeks
Microelectronics Research Center
Georgia Institute of Technology
Atlanta, Georgia 30332

G. C. Fralick
Research Sensor Technology Branch
NASA - Lewis Research Center
Cleveland, Ohio 44135

ABSTRACT

Theoretical expressions are derived for the steady-state frequency response of a supported thermocouple wire. In particular, the effects of axial heat conduction are demonstrated for both a supported one material wire and a two material wire with unequal material properties across the junction. For the case of a one material supported wire, an exact solution is derived which compares favorably with an approximate expression that only matches temperatures at the support junction. Moreover, for the case of a two material supported wire, an analytical expression is derived that closely correlates numerical results.

Experimental data were taken with a type K supported thermocouple. The test thermocouple was constructed with dimensions to demonstrate the effects of axial heat conduction assuming constant physical properties across the junction.

I. INTRODUCTION

The evaluation of jet engine performance and fundamental studies of combustion phenomena depend on the measurement of turbulent fluctuating temperatures of the gas within the engine (Dils and Follansbee, 1976). Historically, these temperatures have been measured with thermocouples. The design of a thermocouple represents a compromise between accuracy, ruggedness and rapidity of response.

For example, the measurement of fluctuating temperatures in the high speed exhaust of a gas turbine engine combustor is required to characterize the local gas density gradients or convective heat transfer (Fralick, 1985). Although thermocouples are suitable for the measurement of high frequency temperature fluctuations (< 1 KHz) in a flowing gas or liquid, the measured signal must be compensated since the frequency of the time dependent fluid temperature is normally much higher than the corner frequency of the thermocouple probe (Scadron and Warshawsky, 1952). Moreover, the amplitude and phase angle of the thermocouple response may be attenuated by axial heat conduction for rugged thermocouples of finite length (Elmore, et al.; 1983, 1986).

In the present study, the theoretical steady-state frequency response of a supported thermocouple wire has been calculated to include the effects of axial heat conduction. These solutions, which represent an extension of earlier work (Forney and Fralick, 1991) are derived for both a supported thermocouple wire

1

with equal physical properties across the junction (e.g., roughly the same thermoconductivity, etc.) and a supported wire with unequal properties across the junction. Solutions are presented in the form of the amplitude ratio and phase angle for both cases.

II. THEORY FOR ONE MATERIAL THERMOCOUPLE

The steady-state frequency response of a thermocouple wire will be developed with the following assumptions: (a) the amplitude of the fluctuating fluid temperature is small relative to the mean absolute temperature (b) the thermocouple dimensions are small relative to the size of the turbulent eddies or enclosure dimensions (c) radial temperature gradients in a wire cross section can be neglected and (d) radiative heat transfer can be neglected relative to conduction and convection.

In this section the geometry of Fig. 1 is considered where the material properties of thermal conductivity k, specific heat c and wire density ρ are assumed to be equal on both sides of the thermocouple junction. If the probe is immersed in a flowing fluid, the expression for the local conservation of energy in the thermocouple wire becomes (Scadron and Warshawsky, 1952)

$$\frac{\partial T_w}{\partial t} = \alpha \frac{\partial^2 T_w}{\partial x^2} + \frac{4h}{\rho c D}\left(T_s - T_w\right)$$

(1)

where $\alpha = k/\rho c$ is the thermal diffusivity of the wire, T_g is the ambient fluid temperature, h is the convective heat transfer coefficient, D is the wire diameter and T_w is the local wire temperature measured along the axis at a distance x from the centerline (Fig. 1.)

The wire and fluid temperatures are measured relative to the mean fluid temperature T_0. The ambient fluid temperature is taken to be a mean temperature together with a sinusoidal varying deviation from the mean,

$$T_e(t) = T_0 + T_f e^{i\omega t} \tag{2}$$

where ω is the angular frequency of the ambient temperature. Since Eq. (1) is linear, we now seek a solution for the local wire temperature of the form (Hildebrand, 1976)

$$T_w = T_0 + \vec{T}_\omega(x)e^{i\omega t}. \tag{3}$$

Referencing all temperatures with respect to the mean gas temperature T_o and normalizing with respect to the amplitude of the fluctuating ambient fluid temperature T_f, one defines a local normalized steady-state frequency response $\vec{T}(x)$ for the thermocouple wire of the form

$$\frac{T_w - T_0}{T_f} = \frac{\vec{T}_\omega(x)e^{i\omega t}}{T_f} = \vec{T}(x)e^{i\omega t}. \tag{4}$$

3

Substituting Eqs. (2) and (3) into Eq. (1), one obtains an ordinary differential equation of the form

$$i\omega T = \alpha \frac{d^2 T}{dx^2} + \omega_n (1 - T) \qquad (5)$$

where $T = \bar{T}(x)$ is the frequency response and the vector notation will be dropped for simplicity. Thus, for the geometry of fig. 1, one seeks a solution to the non-homogeneous linear second order differential equation for the dependent variable T of the form (Forney and Fralick, 1990)

$$\gamma T'' - G(\omega)T = -1. \qquad (6)$$

The general solution to Eq.(6) can be written in the form (Hildebrand, 1976)

$$T(x) = A \sinh qx + B \cosh qx + \frac{1}{G(\omega)} \qquad (7)$$

where the parameters in Eqs. (5) and (6) are defined as

$$\omega_n = \frac{4h}{\rho c D}, \quad \gamma = \frac{\alpha}{\omega_n}, \quad G(\omega) = 1 + i\left(\frac{\omega}{\omega_n}\right) \qquad (8)$$

while in Eq. (7) the constants A and B are complex, $1/G(\omega)$ represents the particular solution and the parameter

4

$$q = \sqrt{\frac{G(\omega)}{\gamma}}.$$

1. Approximate Solution

Assuming that the material properties are constant across the junction and that the wire diameters are D_1 and D_2 in regions 1 and 2, respectively, Eq. (6) is subject to the boundary conditions

$$T_1(l) = T_2(l) = T_a \tag{9a}$$

$$T_2(l+L) = 0 \quad . \tag{9b}$$

In this case, we seek a simple approximate solution that neglects the heat transfer at the interface between regions 1 and 2 at $x = \pm\ l$ where the parameters in Eqs. (5) and (6) are defined in terms of the wire diameters in each region. A similar approach will be used in a later section to obtain an approximate solution for the case in which the material properties of the two elements of the thermocouple are distinctly different. Hence, in region 1

$$\omega_1 = \frac{4h_1}{\rho c D_1}, \qquad \gamma = \frac{\alpha}{\omega_1}, \qquad G_1(\omega) = 1 + i(\frac{\omega}{\omega_1}) \tag{10}$$

where ω_1 is the natural frequency of the wire in region 1 of fig. 1.

5

The solution to Eq. (6) for the one material wire on both sides of the junction in region 1 can be written in the form

$$T_1(x) = A_1 \sinh q_1 x + B_1 \cosh q_1 x + \frac{1}{G_1(\omega)} \, . \tag{11}$$

Substituting $x = \pm l$ in Eq. (11), the boundary conditions in Eq. (9) yield values for the constants

$$A_1 = 0, \quad B_1 = \frac{1}{\cosh q_1 l}\left(T_a - \frac{1}{G_1}\right). \tag{12}$$

Thus, one obtains a steady-state temperature distribution for the wire in region 1 of Fig. 1 in the form

$$T_1(x) = \frac{1}{G_1}\left(1 - \frac{\cosh q_1 x}{\cosh q_1 l}\right) + T_a\left(\frac{\cosh q_1 x}{\cosh q_1 l}\right) \tag{13}$$

We now seek a solution in region 2 that satisfies the boundary conditions of Eq. (9). Since the temperature is symmetric about x = 0, it is convenient to define a continuous steady-state temperature distribution for the large wire of diameter D_2 over the entire region $-(l+L) \leq x \leq (l+L)$ or

$$T_2(x) = \frac{1}{G_2}\left(1 - \frac{\cosh q_2 x}{\cosh q_2(l+L)}\right). \tag{14}$$

6

Since $T_a = T_2(l)$, one obtains the boundary value from Eq. (14)

$$T_a = \frac{1}{G_2}\left(1 - \frac{\cosh q_2 l}{\cosh q_2(l+L)}\right).$$

(15)

Substituting the value for T_a at $x = l$ of Eq. (15) into Eq. (13), the approximate temperature distribution in region 1 becomes

$$T_1(x) = \frac{1}{G_1}\left(1 - \frac{\cosh q_1 x}{\cosh q_1 l}\right) + \frac{1}{G_2}\left(1 - \frac{\cosh q_2 l}{\cosh q_2(l+L)}\right)\frac{\cosh q_1 x}{\cosh q_1 l}$$

(16)

Thus, the approximate frequency response at the thermocouple junction ($x = 0$) for the one material wire becomes

$$T_1(0) = \frac{1}{G_1}\left(1 - \frac{1}{\cosh q_1 l}\right) + \frac{1}{G_2}\left(1 - \frac{\cosh q_2 l}{\cosh q_2(l+L)}\right)\frac{1}{\cosh q_1 l}$$

(17)

The steady-state frequency at the thermocouple junction $x=0$ is normally characterized graphically in the form

$$T(0) = |T(0)|e^{i\Phi}$$

(18)

where $|T(0)|$ is the amplitude ratio and Φ is the phase angle. In the latter case, the phase angle in degrees is

$$\Phi = 57.3 \tan^{-1}\left[\frac{\text{Im } T(0)}{\text{Re } T(0)}\right] \qquad (19)$$

where Im[T(0)] and Re[T(0)] are the imaginary and real parts of T(0), respectively.

2. Exact Solution

If the boundary conditions listed in Eq.(9) include equal rates of conductive heat transfer at the interface between the thermocouple and support wires at $x = \pm \ l$, the exact solution is subject to

$$T_1(l) = T_2(l) \qquad (20a)$$

$$kD_1^2 \frac{dT_1(l)}{dx} = kD_2^2 \frac{dT_2(l)}{dx} \qquad (20b)$$

$$T_2(l+L) = 0 \ . \qquad (20c)$$

Since the solution to Eq. (6) in region 1 is of the form

$$T_1(x) = A_1 \sinh q_1 x + B_1 \cosh q_1 x + \frac{1}{G_1} \qquad (21)$$

8

where by symmetry $T_1(l) = T_1(-l)$, one obtains $A_1 = 0$. Thus, the form of the solution in region 1 becomes

$$T_1(x) = B_1 \cosh q_1 x + \frac{1}{G_1} .$$

$$(22)$$

For region 2, where the spatial coordinate is in the range $l \le x \le (l + L)$, it is convenient to write

$$T_2(x) = A_2 \sinh q_2 (l + L - x) + B_2 \cosh q_2 (l + L - x) + \frac{1}{G_2} .$$

$$(23)$$

From the boundary condition $T_2(l + L) = 0$, one obtains $B_2 = -1/G_2$ or the form of the solution in region 2 becomes

$$T_2(x) = A_2 \sinh q_2 (l + L - x) + \frac{1}{G_2} [1 - \cosh q_2 (l + L - x)] .$$

$$(24)$$

Substituting Eqs. (22) and (23) into boundary condition (20a), one obtains a linear equation for the constants B_1, A_2 or

$$B_1 \cosh q_1 l - A_2 \sinh q_2 L = \frac{1}{G_2} [1 - \cosh q_2 L] - \frac{1}{G_1} .$$

$$(25)$$

Similarly, substituting Eqs. (22) and (23) into boundary condition (20b), one obtains a second linear equation for B_1, A_2 or

9

$$B_1 Q \sinh q_1 l + A_2 \cosh q_2 L = \frac{1}{G_2} \sinh q_2 L \tag{26}$$

where the complex constant Q is defined as

$$Q = \frac{D_1^2 q_1}{D_2^2 q_2} . \tag{27}$$

Solving Eqs. (25) and (26) for B_1 and A_2, one obtains the determinate system

$$B_1 = \frac{\begin{vmatrix} \dfrac{1}{G_2}[1 - \cosh q_2 L] - \dfrac{1}{G_1} & -\sinh q_2 L \\[2mm] \dfrac{1}{G_2}\sinh q_2 L & \cosh q_2 L \end{vmatrix}}{DET} \tag{28}$$

and

$$A_2 = \frac{\begin{vmatrix} \cosh q_1 l & \dfrac{1}{G_2}[1 - \cosh q_2 L] - \dfrac{1}{G_1} \\[2mm] Q \sinh q_1 l & \dfrac{1}{G_2}\sinh q_2 L \end{vmatrix}}{DET} \tag{29}$$

where the determinate in the denominator is equal to

$$DET = \cosh q_1 l \, \cosh q_2 L + Q \sinh q_1 l \sinh q_2 L. \tag{30}$$

Thus, solving for the constants B_1 and A_2 from Eqs. (28) and (29) and substituting

B_1 into Eq. (22), one obtains an exact expression for the steady-state temperature distribution in the form

$$T_1(x) = \frac{\left[\frac{1}{G_2}(\cosh q_2 L - 1) - \frac{1}{G_1}\cosh q_2 L\right]\cosh q_1 x}{\cosh q_1 l \, \cosh q_2 L + Q\sinh q_1 l \, \sinh q_2 L} + \frac{1}{G_1} . \tag{31}$$

Thus, the steady-state frequency response at the thermocouple junction x=0 becomes

$$T(0) = \frac{\frac{1}{G_2}(\cosh q_2 L - 1) - \frac{1}{G_1}\cosh q_2 L}{\cosh q_1 l \, \cosh q_2 L + Q\sinh q_1 l \, \sinh q_2 L} + \frac{1}{G_1} . \tag{32}$$

III. THEORY FOR TWO MATERIAL THERMOCOUPLE

Certain types of thermocouples have distinctly different material properties across the junction. For example, a copper-constantan thermocouple has a thermal conductivity on the copper side that is more than an order of magnitude larger than constantan. In this case, the expressions developed in the previous section for the frequency response are in error since unequal material properties would provide an asymmetric temperature profile.

Referring to fig. 2, the thermocouple schematic now has four distinct regions that are distinguished by either different wire diameters or physical properties. For example, on the left side of the schematic of fig. 1 the thermal conductivity, density

11

and specific heat have the values k_1, ρ_1 and c_1, respectively, while on the right side of the schematic the material properties are k_2, ρ_2 and c_2.

1. Temperature Distribution for Small Wire

Since the differential equation describing the steady-state frequency response Eq. (6) applies to all regions of the schematic of fig. 1, the steady-state frequency response in regions 1 and 2 are given, respectively, by the expressions

$$T_1(x) = A_1 \sinh q_1 x + B_1 \cosh q_1 x + \frac{1}{G_1} \tag{33}$$

$$T_2(x) = A_2 \sinh q_2 x + B_2 \cosh q_2 x + \frac{1}{G_2}. \tag{34}$$

Here, the four constants designated by A and B in Eqs. (33) and (34) are determined by the four boundary conditions

$$T_1(0) = T_2(0) \tag{35a}$$

$$k_1 D_1^2 \frac{dT_1(0)}{dx} = k_2 D_1^2 \frac{dT_2(0)}{dx} \tag{35b}$$

$$T_1(-l) = T_a \tag{35c}$$

$$T_2(l) = T_b . \tag{35d}$$

12

Solving for the four values of the constants designated by A and B in Eqs. (33) and (34), one obtains an expression for the steady-state temperature distribution in region 1 of the form

$$T_1(x) = \frac{1}{G_1} + \left\{ \sinh q_1(x+l) \left[\left(\frac{1}{G_2} - \frac{1}{G_1} \right) \cosh q_2 l + \left(T_b - \frac{1}{G_2} \right) \right] \right.$$

$$\left. + \left(T_a - \frac{1}{G_1} \right) \left[Q_t \cosh q_1 x \sinh q_2 l - \sinh q_1 x \cosh q_2 l \right] \right\} \left(\frac{1}{\Delta_1} \right) \qquad (36a)$$

and in region 2

$$T_2(x) = \frac{1}{G_2} + \left\{ -Q_t \sinh q_2(l-x) \left[\left(\frac{1}{G_2} - \frac{1}{G_1} \right) \cosh q_1 l - \left(T_a - \frac{1}{G_1} \right) \right] \right.$$

$$\left. + \left(T_b - \frac{1}{G_2} \right) \left[\cosh q_2 x \sinh q_1 l + Q_t \cosh q_1 l \sinh q_2 x \right] \right\} \left(\frac{1}{\Delta_1} \right) . \qquad (36b)$$

Here, it should be noted that the two functions above can be obtained from each other by interchanging the subscripts 1 and 2, the values a and b and by changing the sign of x. Also, in Eqs. (36a) and (36b) the parameters

$$\Delta_1 = Q_t \cosh q_1 l \sinh q_2 l + \cosh q_2 l \sinh q_1 l$$

and

$$Q_t = \frac{k_1 q_1}{k_2 q_2} .$$

13

2. Temperature Distribution for Large Wire

In this section a solution is sought for the large wire in regions 3 and 4 of the schematic of fig. 2. To simplify the analysis, a continuous solution is derived for the steady-state frequency response over the entire region $-(l+L) \leq x \leq (l+L)$. This solution must satisfy the boundary conditions

$$T_3(0) = T_4(0) \tag{37a}$$

$$k_1 D_3^2 \frac{dT_3(0)}{dx} = k_2 D_3^3 \frac{dT_4(0)}{dx} \tag{37b}$$

$$T_3(-l - L) = 0 \tag{37c}$$

$$T_4(l + L) = 0. \tag{37d}$$

In principle, it is now possible to derive a continuous solution for $T_3(x)$ over the range $-(l+L) \leq x \leq 0$ and for $T_4(x)$ over the range $0 \leq x \leq (l+L)$. These solutions are obtained from Eqs. (36a) and (36b) by replacing the subscripts $1 \rightarrow 3$ and $2 \rightarrow 4$ and by redefining the parameters $l \rightarrow l + L$ and setting the boundary conditions $T_a = T_b = 0$. Moreover, the boundary condition $T_a = T_3(-l)$ is obtained from the resulting expression for $T_3(x)$ by substituting $x = -l$ while the boundary condition $T_b = T_4(l)$. Thus, one obtains values for T_a, T_b that appear in Eqs. (36a) and (36b) in the form

14

$$T_a = \frac{1}{G_3} + \left\{ \sinh q_3 L \left[\left(\frac{1}{G_4} - \frac{1}{G_3} \right) \cosh q_4 (l+L) - \frac{1}{G_4} \right] \right.$$

$$\left. - \frac{1}{G_3} \left[Q_s \cosh q_3 l \sinh q_4 (l+L) + \cosh q_4 (l+L) \sinh q_3 l \right] \right\} \left(\frac{1}{\Delta_2} \right) \qquad (38)$$

and

$$T_b = \frac{1}{G_4} + \left\{ Q_s \sinh q_4 L \left[\left(\frac{1}{G_3} - \frac{1}{G_4} \right) \cosh q_3 (l+L) - \frac{1}{G_3} \right] \right.$$

$$\left. - \frac{1}{G_4} \left[\cosh q_4 l \sinh q_3 (l+L) + Q_s \cosh q_3 (l+L) \sinh q_4 l \right] \right\} \left(\frac{1}{\Delta_2} \right). \qquad (39)$$

Here, the parameters are defined as

$$\Delta_2 = Q_s \cosh q_3 (l+L) \sinh q_4 (l+L) + \cosh q_4 (l+L) \sinh q_3 (l+L)$$

and

$$Q_s = \frac{k_1 q_3}{k_2 q_4} \, .$$

3. Frequency Response

The steady-state frequency response for the two material supported thermocouple is obtained from Eq. (36a) or (36b) by setting x = 0:

15

$$T(0) = \frac{1}{\Delta_1}\left\{Q_1\sinh q_2 l\left[T_a + \frac{1}{G_1}(\cosh q_1 l - 1)\right] + \sinh q_1 l\left[T_b + \frac{1}{G_2}(\cosh q_2 l - 1)\right]\right\} \qquad (40)$$

where T_a and T_b are given by Eqs. (38) and (39).

It should be noted that the steady-state frequency response Eq. (40) provides a wire temperature that is continuous everywhere and conserves the heat flux at the junction x = 0. This represents an approximate solution since the heat flux at the interface between the large and small wires $x = \pm l$ has been neglected.

IV. RESULTS

The amplitude ratio and phase angle of the thermocouple frequency response were plotted graphically for the case of a one material wire as shown in the schematic of fig. 1. In this case, average properties of a type B or $Pt/6\% Rh - Pt/30\% Rh$ were used since the material properties were nearly equal across the thermocouple junction. The wire dimensions, properties and gas conditions are listed in table 1(Touloukian et al., 1970).

The amplitude ratio and phase angle were also plotted for a two material thermocouple wire as shown in the schematic of fig. 2. In this case, a type B thermocouple described in table 1 was used in addition to a type T or copper - constantan described in table 2 (Touloukian et al., 1970).

The form of the convective heat transfer coefficient h that appears in the

computation of the natural frequency ω_n defined in Eq. (8) was determined from the expression (Scadron and Warshawsky 1952)

$$Nu = .485 \, Re^{\frac{1}{2}} Pr^{\frac{1}{3}} \tag{41}$$

where $Nu \, (= hD / k_f)$ is the Nusselt number, k_f is the thermal conductivity of the ambient fluid, $Pr(= v_f / \alpha)$ is the Prandl number, and $Re \, (= v \, D / v_f)$ is the Reynolds number of the thermocouple wire. Here, v and v_f are the fluid velocity and kinematic viscosity, respectively. It should be noted that the convective heat transfer coefficient $h \; \alpha \; D^{1/2}$ and the natural frequency of a thermocouple wire for given material properties $\omega_n \; \alpha \; D^{-3/2}$.

1. One Material Thermocouple

The amplitude ratio $|T(0)|$ at the wire junction for the steady-state frequency response derived from Eqs. (17) and (32) is shown in fig. 3. This assumes a type B thermocouple wire with the dimensions listed in table 1. In this case, the average material properties listed in table 1 were used since the one material theory assumes that the properties of the thermocouple wire are uniform across the junction. It is evident in fig. 3 that the amplitude ratio derived from the approximate expression Eq. (17) is nearly identical to the exact derivation Eq. (32). Thus, it appears that the conservation of heat flux at the interface between the small and large wires of the schematic of fig. 1 is of secondary importance.

Also included in fig. (3) are the numerical computations of Stocks (1986).

These solutions represent explicit finite difference solutions to the one dimensional unsteady heat transfer equation as shown in Eq. (1). The small deviation of the numerical results from the exact solution at low frequency in fig. (3) is apparently due to the unsteady character of the numerical results. Similar computations of the phase angle Φ for the type B thermocouple are represented in fig. 4. As indicated, the phase angle varies over the range $0 \geq \Phi \geq -\pi/2$ and approaches the lower limit of $-\pi/2$ for large frequencies $\omega/\omega_n \gg 1$.

The spacial variation of the amplitude ratio $|T(x)|$ derived from Eqs. (17) and (32) is graphed in fig. 5. These computations were made at an angular frequency of $\omega/\omega_n = 0.1$ for the type B thermocouple. As evident in fig. 5, the difference between the exact and approximate expression is somewhat exaggerated at a very low frequency. Nevertheless, the error represented by the approximate solution is less than 7% over the length of the thermocouple. As stated earlier, matching the heat flux at the interface between the small and large wire at $x = \pm l$ in the schematic of fig. 1 appears to be of secondary importance in relation to providing a continuous temperature profile along the wire.

The amplitude ratio $|T(0)|$, phase angle Φ and spacial variation $|T(x)|$ are also plotted in figs. (6), (7) and (8), respectively, from the steady-state frequency response represented by Eqs. (17) and (32). These results represent a type B thermocouple with a smaller diameter ratio $D_2/D_1 = 2$ (see table 1 for dimensions). As indicated in figs. (6), (7) and (8), the approximate and exact solutions represent comparable results in all three cases. Thus, the diameter ratio of the large and small wire

18

appears to have little effect in the favorable comparison between the approximate and exact solutions representing the one material steady-state frequency response.

2. Two Material Thermocouple

The amplitude ratio $|T(0)|$ at the wire junction for the steady-state frequency response derived from Eqs. (17) and (40) is shown in fig. 9. This assumes a type B thermocouple wire with the dimensions listed in table 2. In this case, the average material properties listed in Table 2 were used for the amplitude of the frequency response derived from the one material solution of Eq. (17). Also plotted in fig. 9 is the amplitude ratio derived from the two material solution of Eq. (40). In the latter case, the individual material properties listed in Table 2 were used.

As expected, the amplitude ratio for the steady-state frequency response of a type B thermocouple is nearly identical with either the one material or two material approximate solutions. This is a consequence of roughly equal material properties across the junction for type B thermocouples. This plot also validates the two material approximate solution Eq. (40) and the values of the boundary conditions for T_a and T_b substituted from Eqs (38) and (39). The same conclusion can be drawn with respect to the phase angle Φ, shown in fig. 10.

The spacial variation of the amplitude ratio $|T(x)|$ derived from Eqs. (17) and (40) is plotted in fig. 11. These computations were made at an angular frequency of $\omega/\omega_n = 0.1$ for the type B thermocouple with the dimensions listed in table 2. It is

19

interesting to note the small asymmetry in the amplitude ratio on the left and right side of the junction. This asymmetry is the result of the small differences in the physical properties across the junction as listed in table 2.

The steady state amplitude ratio $|T(0)|$ for a type T thermocouple is plotted in fig. 12 using equations (17) and (40). The dimensions and material properties are listed in table 2. The average material properties listed in Table 2 were used to compute the amplitude ratio of the frequency response with the one material solution, Eq. (17). Also plotted in fig. 12 is the amplitude ratio derived from the two material solution, Eq. (40). In the latter case, the individual material properties also listed in table 2 were used.

As indicated in fig. 12, the amplitude ratio for the approximate one material steady-state frequency response of a type T thermocouple is distinctly different from the two material approximate solution. This is a consequence of unequal material properties across the junction for the type T thermocouple. Also shown in fig. 12 is a numerical solution of the second order ordinary differential equation for the temperature, Eq. (6). The numerical finite difference solution of the boundary value problem of Eq. (6) matches both the temperature and heat flux at x = 0 and $x = \pm l$ in the schematic of fig. 2. It is clear from fig. 12 that the approximate two material analytical solution, equation (40), is in good agreement with the numerical results despite some differences at low frequencies $\omega/\omega_1 < .04$. Similar results are indicated for the phase angle ϕ in fig. 13.

The spacial variation of the amplitude ratio $|T(x)|$ derived from Eqs. (17) and

(40) is graphed in fig. 14. These computations were made at an angular frequency of $\omega/\omega_1 = 0.1$ for the type T thermocouple. As evident in fig. 14, the two material solution derived from Eq. (40) accurately represents the features of the asymmetry associated with a type T thermocouple. In particular, the relatively large resistance to axial heat conduction in the constantan wire on the right of the junction is reflected in the larger values of the amplitude ratio $|T(x)|$. Also shown in fig. 14 is the approximate one material solution represented by Eq. (17). In the latter case, the average values for the material properties of a type T thermocouple were used as listed in Table 2. Therefore, one can conclude that for thermocouples whose material properties on either side of the junction are markedly different, the two material solution developed in this paper is a substantial improvement in accuracy both in frequency response and in temperature distribution along the wire.

V. Experimental Procedure

In the experiment described below, thermocouple sensors were exposed to a constant velocity air stream of varying temperature. In particular, the dynamic response of the thermocouple sensors to a square wave temperature profile was measured for a range of frequencies.

1. Rotating Wheel Experiment

A rotating wheel configuration was used to deliver the test airstream to the proposed sensors. A similar experimental apparatus is described in detail by

21

Elmore et al. (1986). A schematic of the rotating wheel apparatus used in the present experiment is shown in figure 15. As the wheel rotates, the holes pass the two air supply tubes which allow slugs of hot and cold air to alternately enter a transition tube assembly mounted directly above the rotating wheel. In the transition tube the slugs of hot and cold air coalesce into a single air stream providing roughly a square wave temperature profile covering a range of frequencies from roughly 1 to 30 Hz.

The analog temperature signal was digitized with a Data Translation DT-2801 board mounted in an expansion slot of an IBM AT compatible computer as shown in figure 15. The ASYST software loaded on the hard disc of the personal computer provided a flexible system for data storage, manipulation and display.

The true temperature profile of the airstream was measured with a constant current anemometer (TSI 1054-A) and sensor (1226 PI 2.5).

2. Thermocouple Construction

Thermocouple wire of the desired length and type is threaded into the four hole ceramic with the thermocouple end last. Three or four kinks are made in each wire near the thermocouple end so the wire must be firmly pulled into the tube leaving enough wire sticking out to make the thermocouple. Drops of epoxy are picked up with a piece of .010" diameter wire, added to the ceramic tube at A (see fig. 16) and pushed down around both wires. The kinks and epoxy firmly fasten the wires in the ceramic so they do not twist when the free ends are

22

manipulated for electrical connections.

The junction at B in figure 16 is made by cutting the large wire about half way through with a razor blade, laying the small diameter wire in the cut, and welding the cut closed with a stored energy spot welder. After the weld, the excess wire ends that protrude through the weld area are bent and broken off to clean up the junction.

For the chromel alumel couples, the junction at C of figure 16 was made using a stored energy spot welder. The wires are crossed and welded and then trimmed with a razor blade and bent with tweezers under a microscope until collinear.

A stored energy spot welder will not work for the copper constantan couples. For these couples the junctions were made by silver soldering. The silver solder wire is coated with flux and the end heated with a torch until a drop forms. A twisted pair of thermocouple wires is pushed briefly into the flux coated solder drop. The solder will wet the pair up to where the twist stops. Again using a razor blade and tweezers under a microscope, the thermocouple is bent and trimmed until collinear.

3. ASYST Software

ASYST software was developed to acquire temperature data simultaneously from the thermocouple and constant current anemometer. Data were digitized for two channels at a sampling rate of 512 Hz per channel for a total sample time of

two seconds. The ASYST software code is listed in figure 17.

The ASYST code first plotted the temperature profiles versus time from the thermocouple and anemometer and an example of the plot is shown in figure 18. The ASYST software next took the Fast Fourier Transform of the temperature data in each channel and recorded the amplitude ratio and phase angle between both channels at the first harmonic for the square wave. These data are discussed in the next section.

VI. Results

Initial tests with a signal generator and the output from an RC circuit indicated that the ASYST code and data acquisition hardware were operating properly. Several test sensors were constructed and tested with the dimensions listed in table 3. In each case measurements of the amplitude and phase angle were compared with the appropriate theory. A discussion of the results is given below.

1. First Order Response

The amplitude ratio and phase angle were measured with the type K thermocouple listed first in table 3. The lengths of the thermocouple and support wires in this case were chosen to eliminate the effects of axial heat conduction. The experimental data representing the amplitude ratio are plotted in figure 19 along with the theory representing a first order frequency response. The experimental data were correlated with a natural frequency $\omega_1 = 5.5 \, \text{sec}^{-1}$ and a

24

thermal diffusivity of $\alpha = .059 \, cm^2 / sec.$

As indicated in figure 19 the data has been correlated with the theory to within 10%. Although the experimental data is reproducible, there is a noticeable drift of the data relative to the theory with increasing wheel frequency ω. The drift is probably due to a small increase in the natural frequency ω_1 of the thermocouple wire with increasing wheel frequency ω.

The natural frequency ω_1 of Equation (10) depends on accurate predictions of the convective heat transfer coefficient h from Equation (41). However, there may be a small change in either the mean air velocity or unsteadiness in the mean velocity which would lead to small changes in the heat transfer coefficient h and the natural frequency ω_1.

Also plotted in figure 20 are experimental data representing the phase angle Φ for the first order frequency response of the type K thermocouple. In this case the data is correlated to within 7% of the theory. The experimental data for the phase angle also indicate a small drift in the natural frequency ω_1 as was apparent in figure 19.

2. Frequency Response (one material)

The amplitude ratio and phase angle were measured with the second type K thermocouple listed in table 3. The lengths of the thermocouple and support wires in this case were chosen (i.e., shortened) to demonstrate the effects of axial

heat conduction. The experimental data representing the amplitude ratio are plotted in figure 21 along with the theoretical prediction given by Eq. 32. Both the data and theory were correlated by assuming that the material properties are uniform across the thermocouple junction. In this case the data were correlated with a natural frequency $\omega_1 = 5.0 \, sec^{-1}$ and a thermal diffusivity of

$\alpha = .059 \, cm^2 / sec.$

As indicated in figure 21 the data has been correlated with the theory to within 10% over most of the range of wheel frequencies. The data is reproducible but again a noticeable drift of the experimental data exists relative to the theory as was discussed in the previous section.

Also plotted in figure 22 are experimental data representing the phase angle Φ for the frequency response of the shortened type K thermocouple. The data is correlated to within 7% of the theory. The experimental data for the phase angle also indicate a small drift in the natural frequency ω_1.

IV. NOMENCLATURE

A	=	constant of integration
B	=	constant of integration
c	=	material specific heat $\left(J - gm^{-1} - {^0K^{-1}}\right)$
D	=	thermocouple wire diameter (cm)
G	=	$1 + i\left(\omega / \omega_n\right)$
h	=	heat transfer coefficient $\left(J - cm^{-2} - s^{-1} - {^0K^{-1}}\right)$
i	=	unit imaginary number $\left(= \sqrt{-1}\right)$
k	=	material thermoconductivity $\left(J - cm^{-1} - s^{-1} - {^0K^{-1}}\right)$
k_f	=	gas thermoconductivity $\left(J - cm^{-1} - s^{-1} - {^0K^{-1}}\right)$
l	=	length of small thermocouple wire (cm)
L	=	length of large thermocouple wire (cm)
Nu	=	Nusselt number (= hD/k_f)
Pr	=	Prandl number $\left(= v_f / \alpha\right)$
Q	=	$\dfrac{D_1^2 q_1}{D_2^2 q_2}$
Q_t	=	$\dfrac{k_1 q_1}{k_2 q_2}$
Q_s	=	$\dfrac{k_1 q_3}{k_2 q_4}$
q	=	$\left(G/\gamma\right)^5$
Re	=	Reynolds number $\left(= vD / v_f\right)$
t	=	time (s)

T	$=$	steady-state frequency response
T_f	$=$	amplitude of periodic gas temperature $\left(^{0}K\right)$
T_g	$=$	gas temperature $\left(^{0}K\right)$
T_0	$=$	mean gas temperature $\left(^{0}K\right)$
$\vec{T_\omega}$	$=$	complex amplitude of periodic wire temperature $\left(^{0}K\right)$
T_w	$=$	local wire temperature $\left(^{0}K\right)$
v	$=$	gas velocity $\left(cm-s^{-1}\right)$
x	$=$	axial distance from center of wire (cm)

Greek Symbols

α	$=$	thermal diffusivity $\left(cm^2-s^{-1}\right)$
γ	$=$	α/ω_n $\left(cm^2\right)$
υ_f	$=$	kinematic viscosity of gas $\left(cm^2-s^{-1}\right)$
ω	$=$	angular frequency $\left(s^{-1}\right)$
ω_n	$=$	natural frequency of wire $\left(=4h/\rho cD\right)\left(s^{-1}\right)$
Φ	$=$	phase angle
ρ	$=$	material density $\left(gm - cm^{-3}\right)$
Δ_1	$=$	dimensionless function
Δ_2	$=$	dimensionless function

V. REFERENCES

1. Carslaw, H. S., Introduction to the Mathematical Theory of the Conduction of Heat in Solids, Dover Publications, 2nd edition (1945).

2. Dils, R. R. and Follansbee, P. S., Wide Bandwidth Gas Temperature Measurements in Combustor and Combustor Exhaust Gases, Instrumentation in the Aerospace Industry, 21 (B. Washburn, ed.), ISA 76245 (1976).

3. Elmore, D. L., Robinson, W. W. and Watkins, W. B., Dynamic Gas Temperature Measurement System: Final Report, NASA CR-168267 (1983).

4. Elmore, D.L., Robinson, W. W. and Watkins, W. B., Further Development of the Dynamic Gas Temperature Measurement System: Vol. I - Technical Efforts, NASA CR-179513 (1986).

5. Stocks, D. R., Further Development of the Dynamic Gas Temperature Measurement System: Vol. II - Computer Program User's Manual, NASA CR-179604 (1986).

6. Forney, L. J. and Fralick, G. C., Frequency Response of a Uniform Thermocouple Wire: Effects of Axial Conduction, Proceedings of the 6th Miami International Symposium on Heat and Mass Transfer (1990).

7. Fralick, G. C., Correlation of Velocity and Velocity-Density Turbulence in the Exhaust of an Atmospheric Burner, Turbine Engine Hot Section Technology - 1985, NASA CP-2465, pp. 81-85.

8. Forney, L. J. and Fralick, G. C., Frequency Response of a Thermocouple Wire: Effects of Axial Heat Conduction (submitted, International J. Heat and Mass Transfer, 1991).

9. Hildebrand, F. B., Advanced Calculus for Applications, (2nd Ed), Prentice - Hall (1976).

10. Scadron, M.D. and Warshawsky, I., Experimental Determination of Time Constants and Nusselt Numbers for Bare-Wire Thermocouples in High-Velocity Air Streams and Analytic Approximation of Conduction and Radiation Errors, NACA TN-2599 (1952).

11. Touloukian, Powell, Ho and Clemens, (ed.), Thermal Physical Properties of Matter, Purdue Research Foundation, Plenum Pub. (1970).

Table 1 - Properties of One Material Wire (Type B)

<u>Dimensions (cm)</u>

$\underline{D_1}$	$\underline{D_2}$	$\underline{D_2/D_1}$	$\underline{1}$	$\underline{L}$
.025	.05	2	.2	.35
.0076*	.038	5	.1	.2

<u>Average Properties of Type B</u>

$\rho c \left(\dfrac{J}{cm^3 - {}^{\circ}K} \right)$	$\alpha \left(\dfrac{cm^2}{sec} \right)$
3.8	.22

<u>Gas Properties</u>

$T_0 = 900\,{}^{\circ}K$

$M = .26$

$P = 1\,atm$

$*\,\omega_1 = 32.9\ sec^{-1}$

Table 2 - Properties of Two Material Wire

Dimensions (cm)

D₁	D₂	D₂/D₁	l	L
D_1	D_2	D_2/D_1	l	L
.0076	.038	5	.1	.2

Air Properties

$T_0 = 300\ °K$

$P = 1\ atm$

$V = 50\ m/sec$

Properties of Type B

	$\rho c \left[\dfrac{J}{cm^3 - ok}\right]$	$\alpha \left[\dfrac{cm^2}{sec}\right]$
Pt - 6% Rh	2.73	.238
Pt - 30% Rh	2.86	.190
Average	2.8	.214

Properties of Type T

	$\rho c \left[\dfrac{J}{cm^3 - °K}\right]$	$\alpha \left[\dfrac{cm^2}{sec}\right]$
Copper	3.44	1.16
Constantan	3.48	.067
Average	3.46	.614

Wire Location

Region	Type B	Type T
1	Pt - 6% Rh	Copper
2	Pt - 30% Rh	Constantan

31

Table 3 - Dimensions for Test Thermocouples (cm)

Test	Thermocouple Type	D_1	D_2	D_2/D_1	l	L
First Order	K	.0076	.038	5	0.25	0.5
Axial Conduction (one material)	K	.0076	.038	5	0.1	0.2
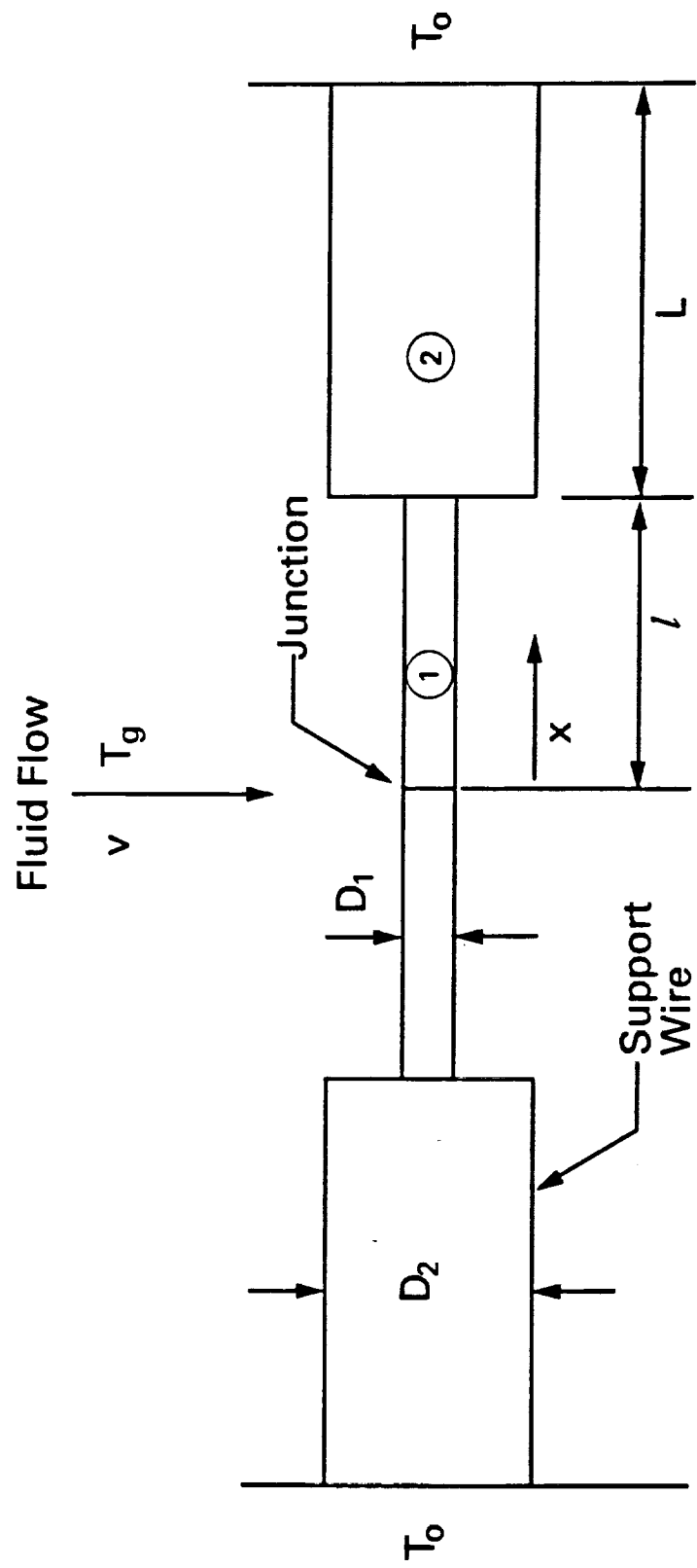
1. Schematic of one material supported wire.
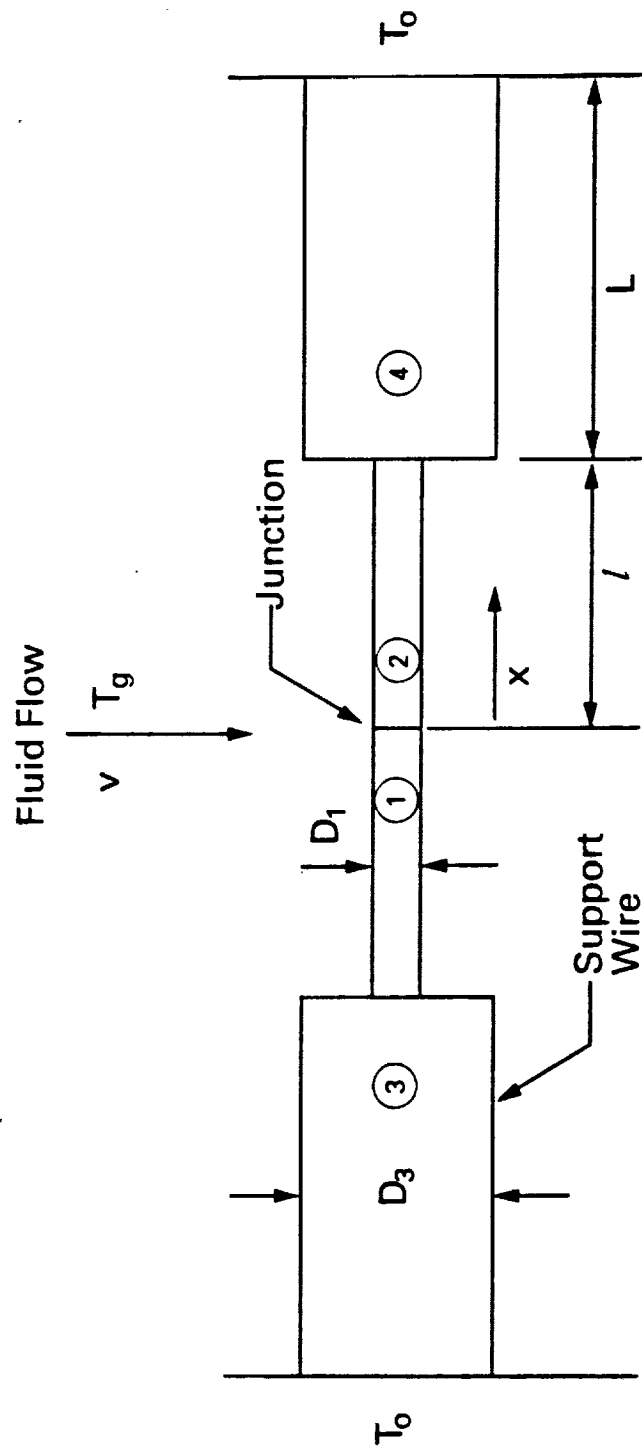
2. Schematic of two material supported wire.
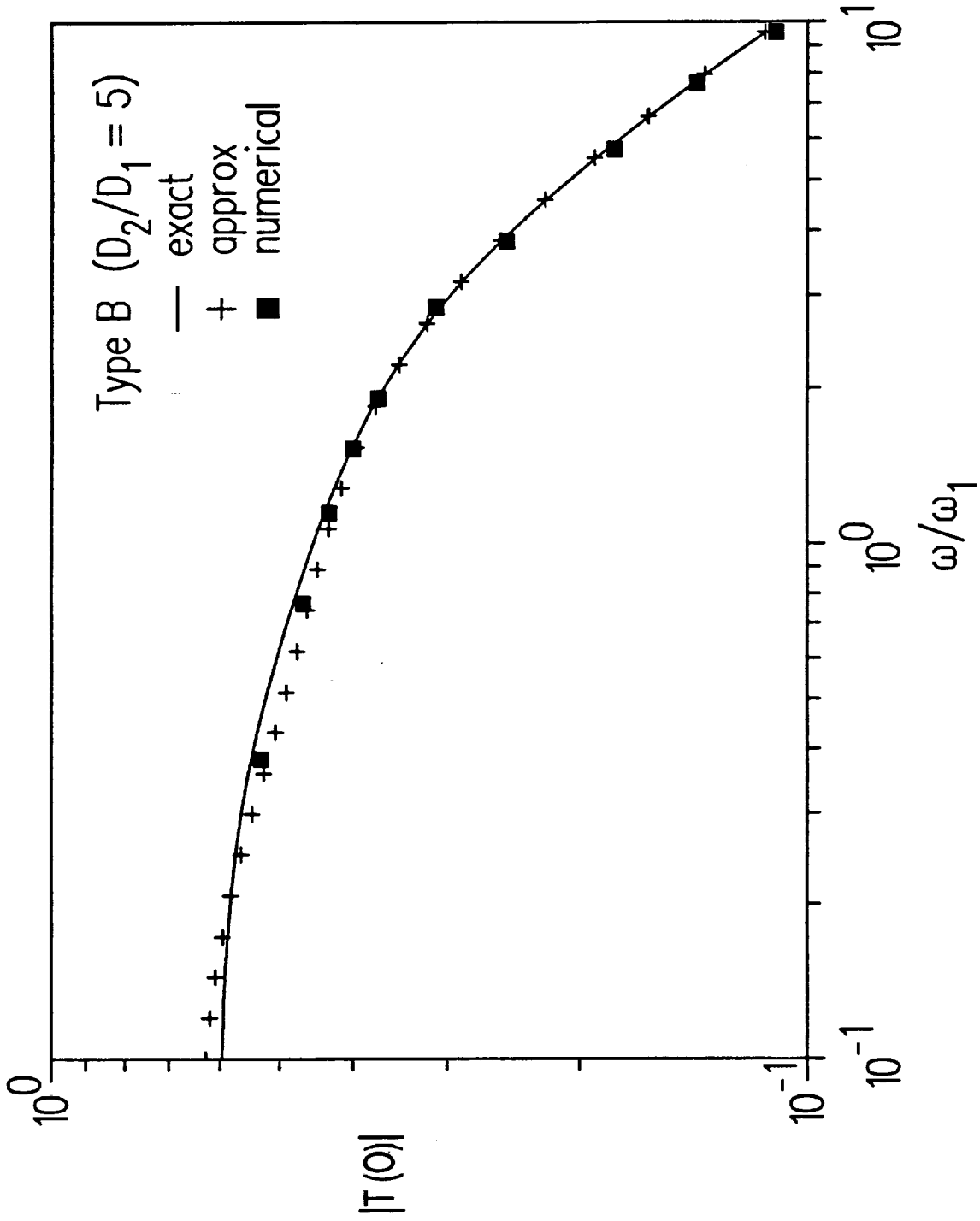
3. Amplitude ratio vs. angular frequency for one material wire. Solid line is exact solution Eq. (17). Crosses are approximate solution Eq. (32); Solid line is exact solution Eq. (17).

4. Phase angle vs. angular frequency for one material wire. Solid line is exact solution Eq. (32); Crosses are approximate solution Eq. (17).

Type B $(D_2/D_1 = 5 , \omega/\omega_1 = .1)$

— exact
+ approx

$\Pi(x)$|

x/(l+L)
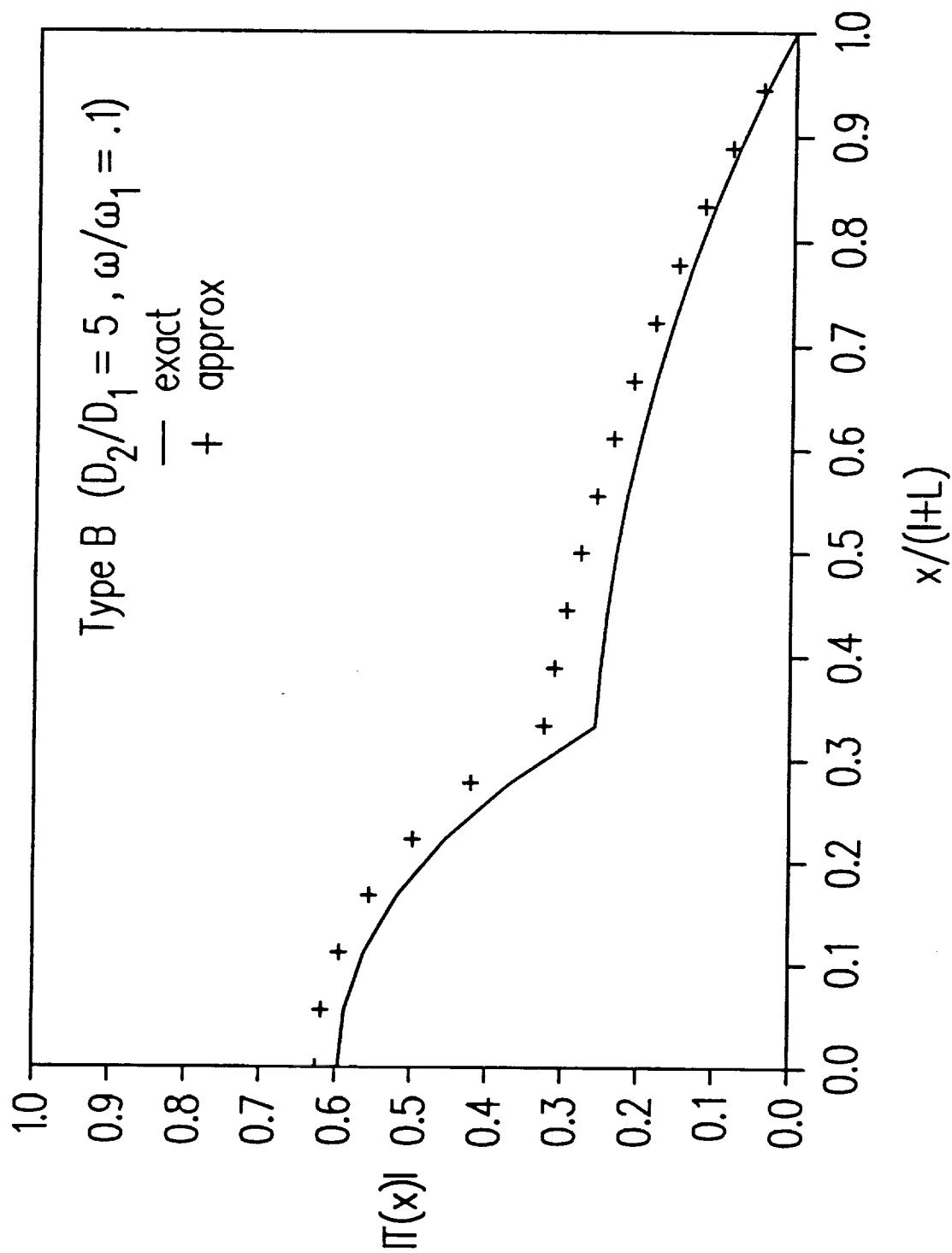
5. Amplitude ratio vs. distance for one material wire. Solid line is derived from Eqs. (14) and (16). Crosses are derived from Eqs. (24) and (31).

37

Type B $(D_2/D_1 = 2)$
— exact
+ approx

$|T(0)|$

ω/ω_1
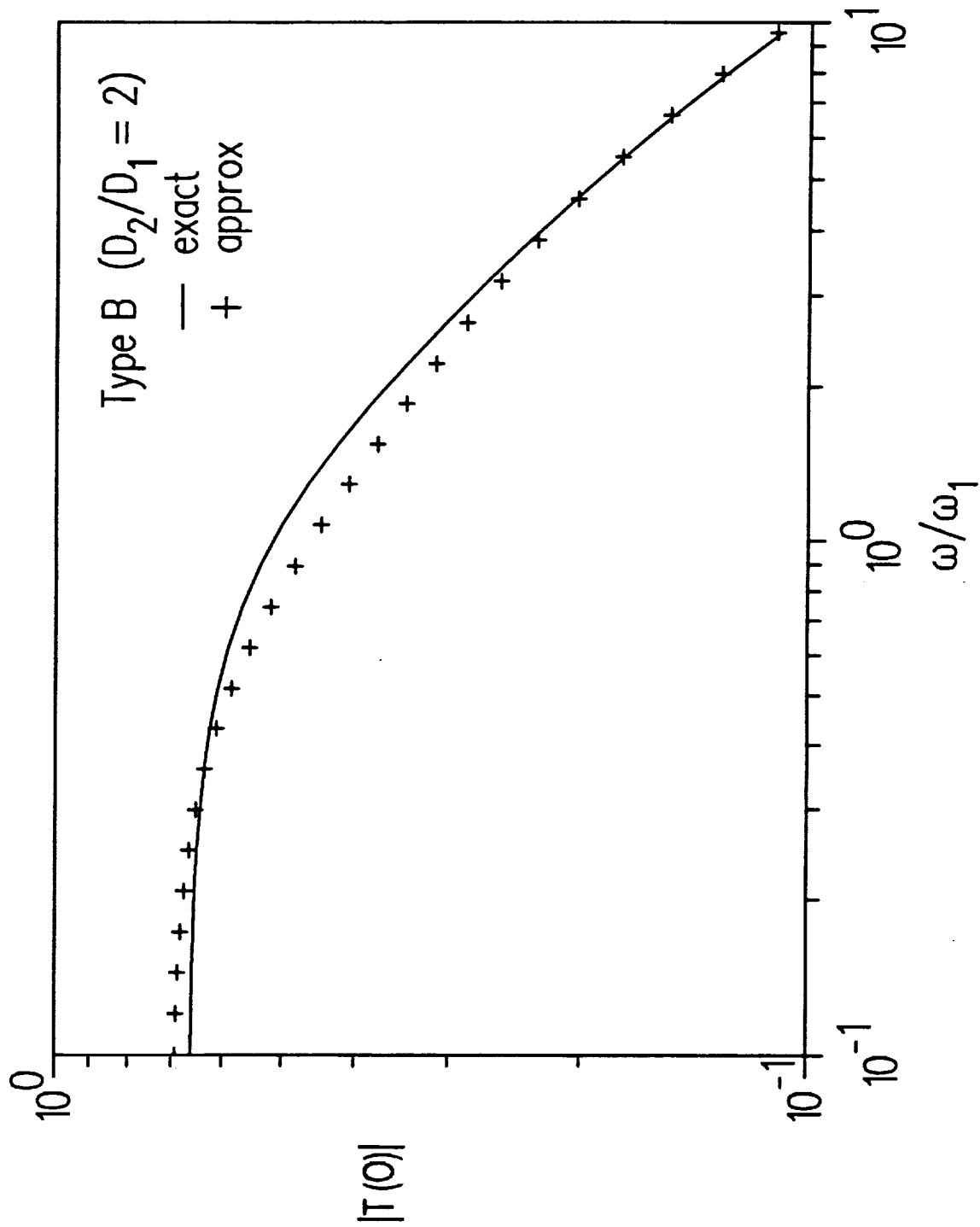
6. Amplitude ratio vs. angular frequency for one material wire. Solid line is Eq. (20). Crosses are Eq. (17).
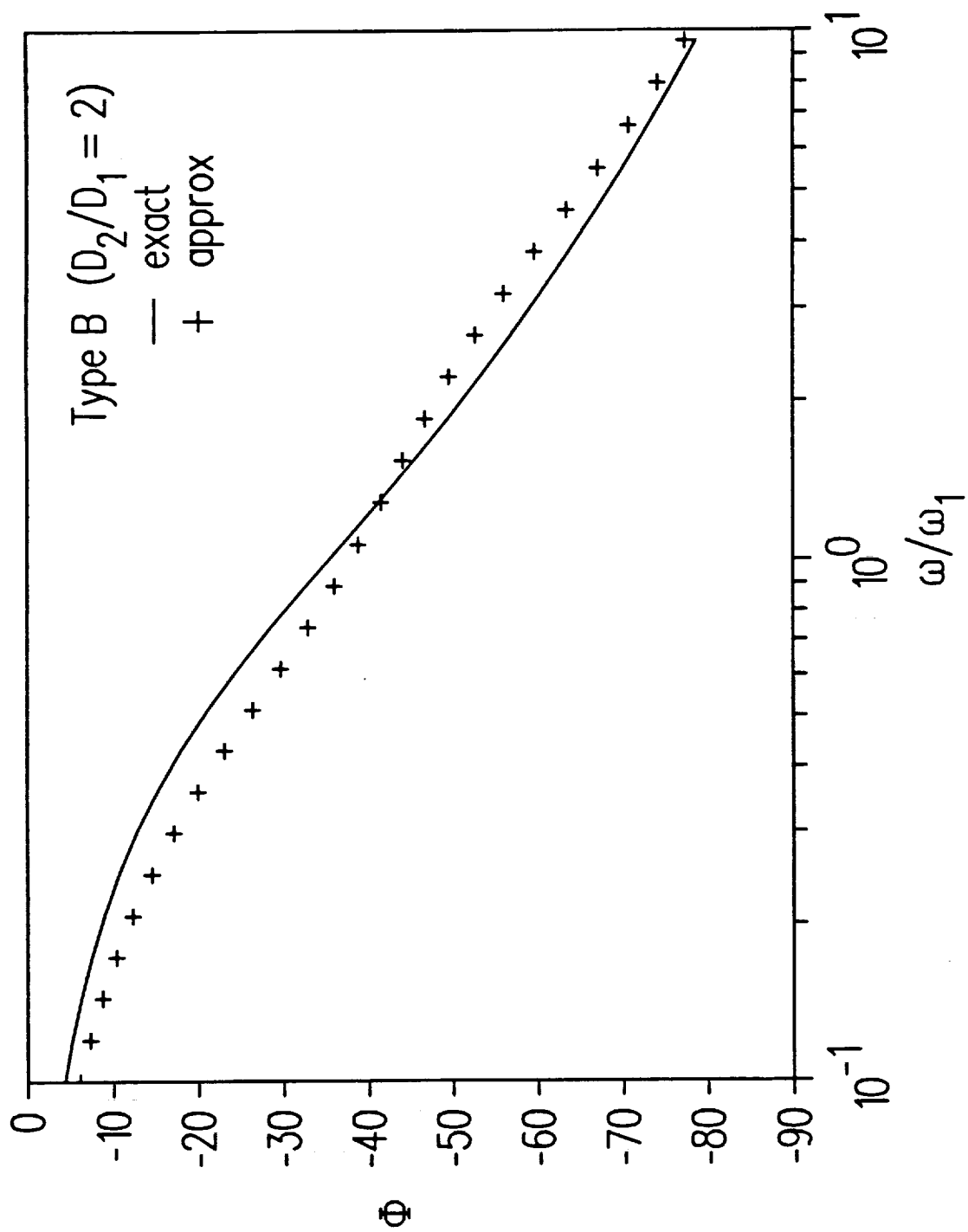
7. Phase angle vs. angular frequency for one material wire. Solid line is Eq. (32). Crosses are Eq. (17).

Type B $(D_2/D_1 = 2, \omega/\omega_1 = .1)$

— exact
+ approx

$\Pi(x)$

x/(l+L)
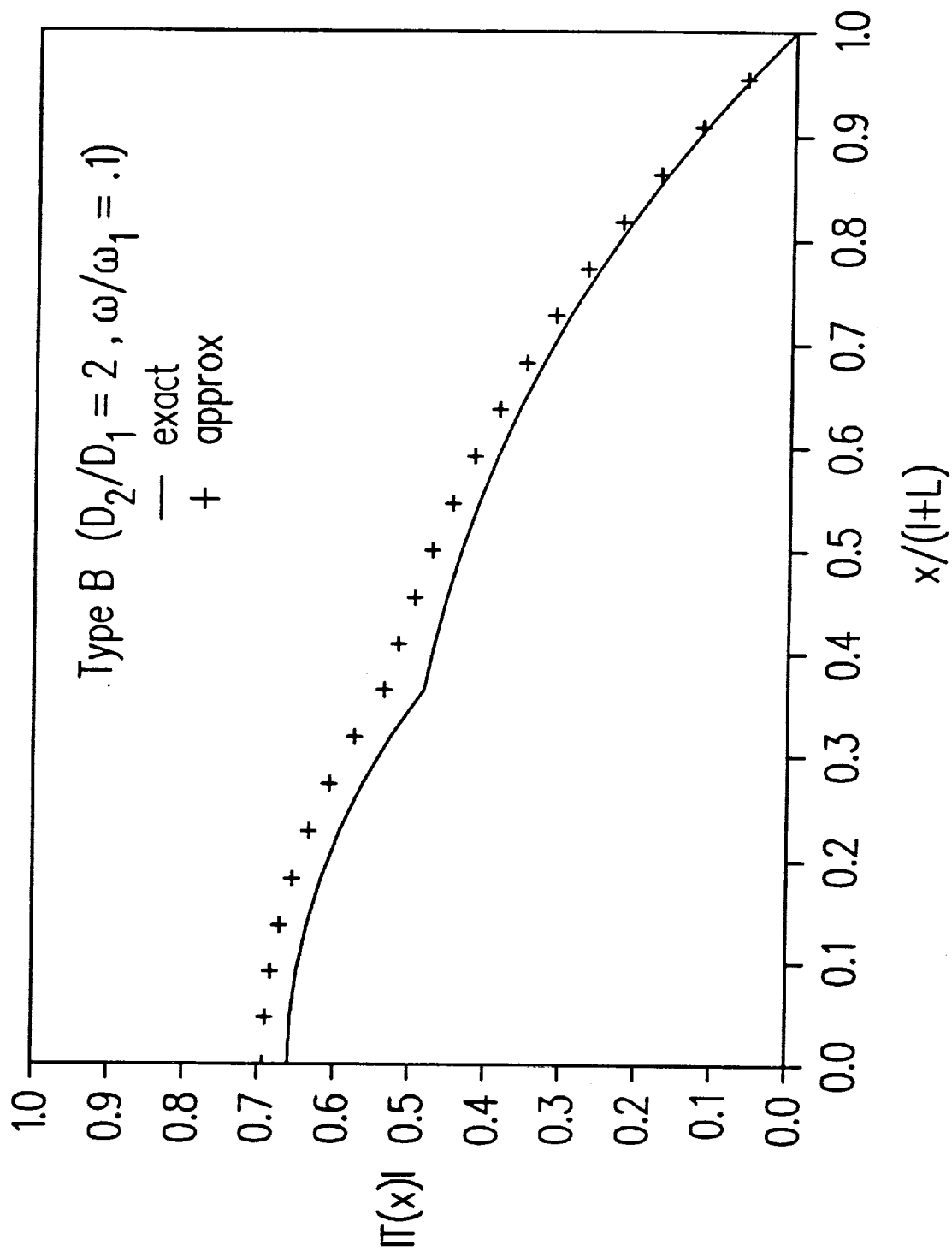
8. Amplitude ratio vs. distance for one material wire. Solid line derived from Eqs. (14) and (16). Crosses are derived from Eqs. (24) and (31).

40
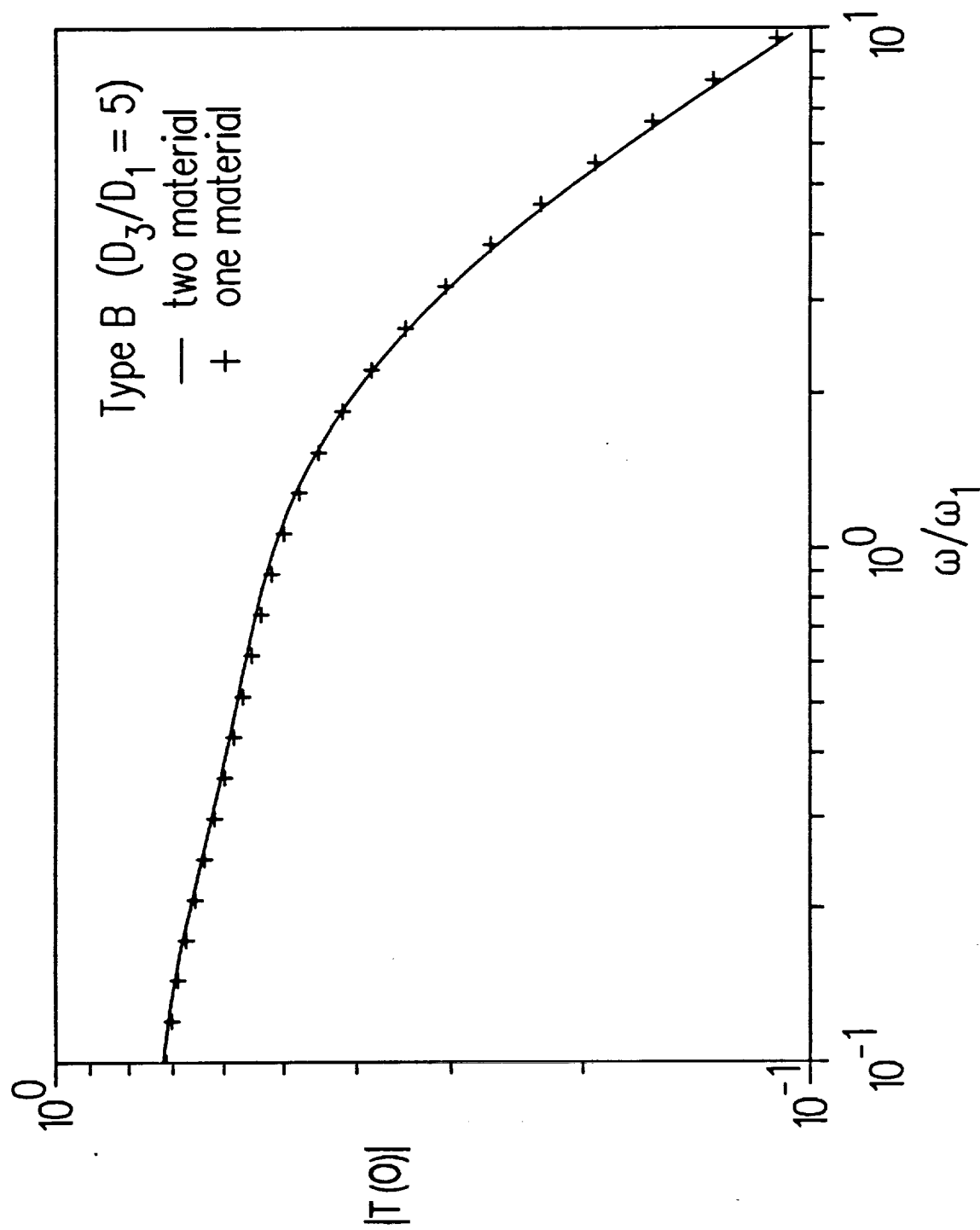
9. Amplitude ratio vs. angular frequency for two material wire. Solid line is Eq. (40). Crosses are approximate one material solution Eq. (17).
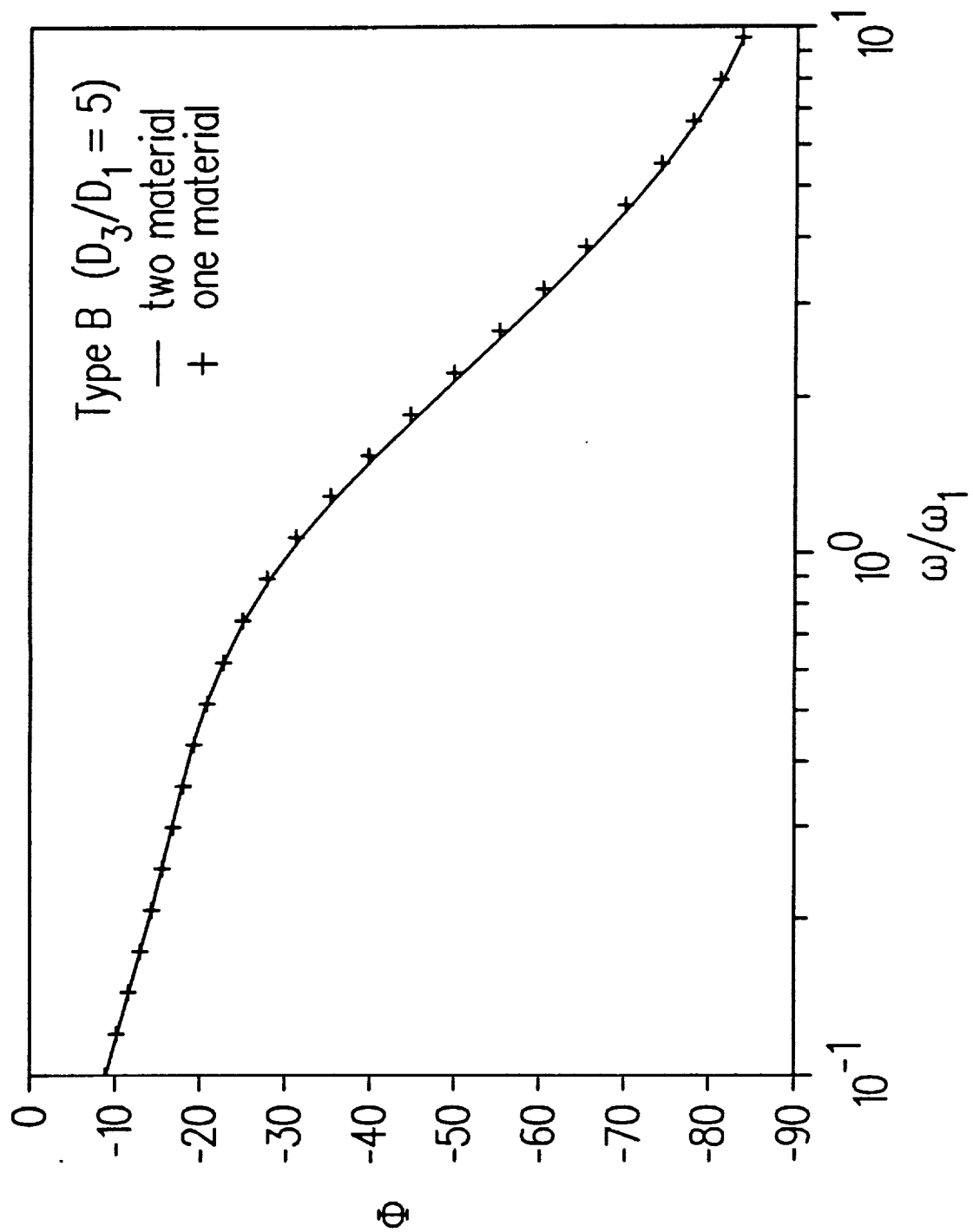
10. Phase angle vs. angular frequency for two material wire. Solid line is Eq. (40). Crosses are approximate one material solution Eq. (17).
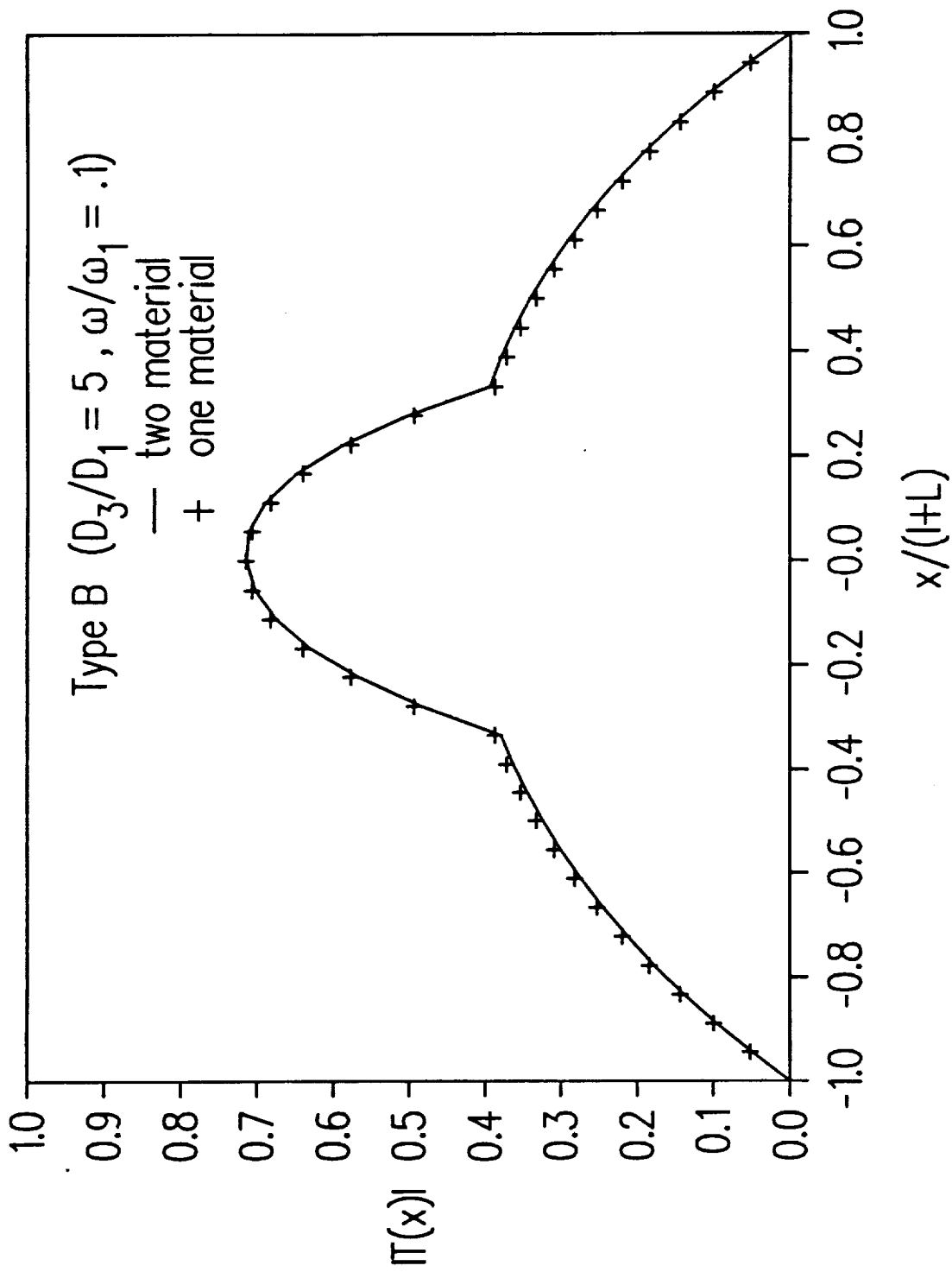
11. Amplitude ratio vs. distance for two material wire. Solid line derived from Eqs. (36a) and (36b). Crosses are approximate one material solution Eqs. (14) and (16).

43
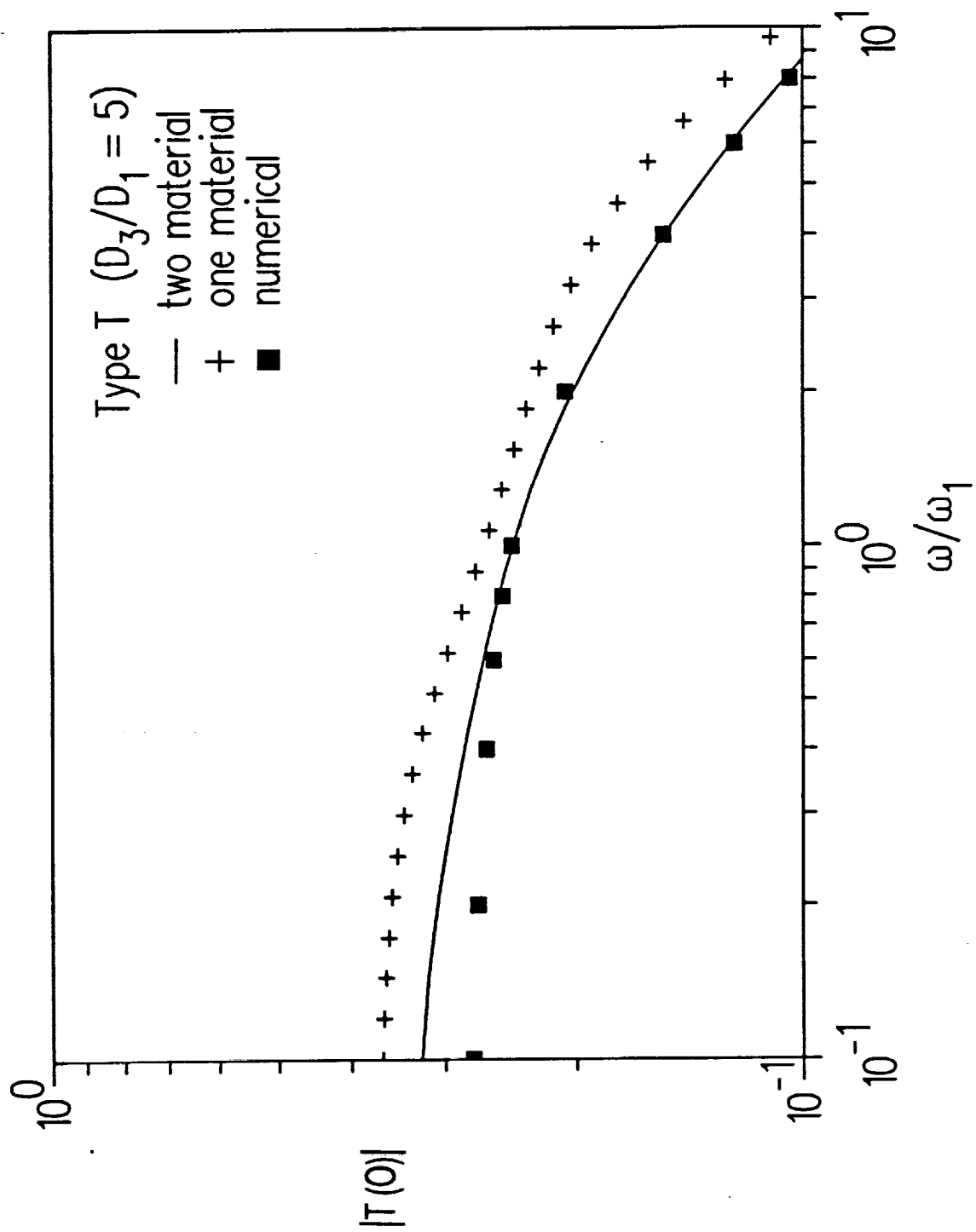
12. Amplitude ratio vs. angular frequency for two material wire. Solid line is Eq. (40). Crosses are approximate one material solution Eq. (17).
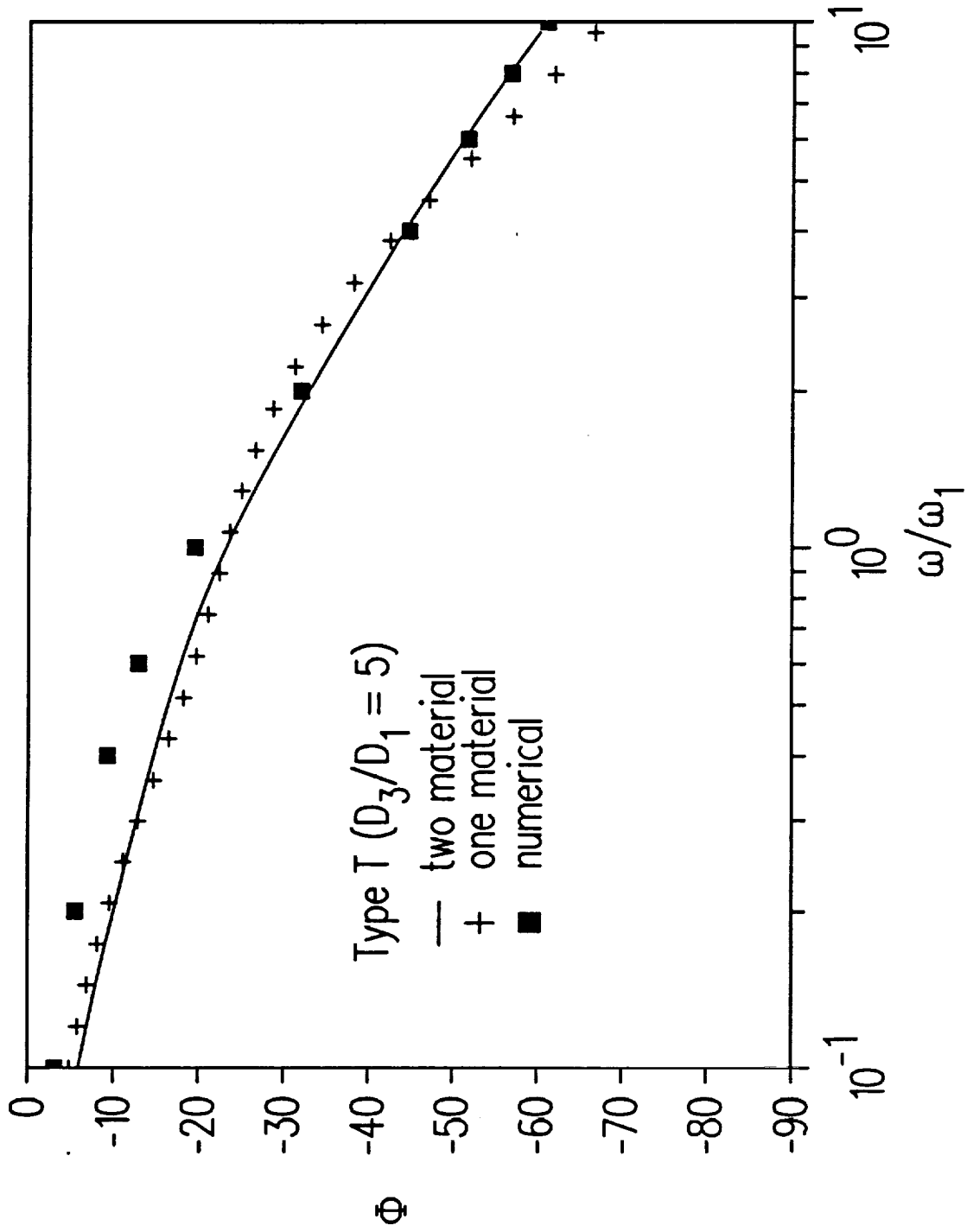
13. Phase angle vs. angular frequency for two material wire. Solid line is Eq. (40). Crosses are approximate on material solution Eq. (17).

Type T ($D_3/D_1 = 5$, $\omega/\omega_1 = .1$)

— two material
+ one material
■ numerical

$|\Pi(x)|$

x/(l+L)
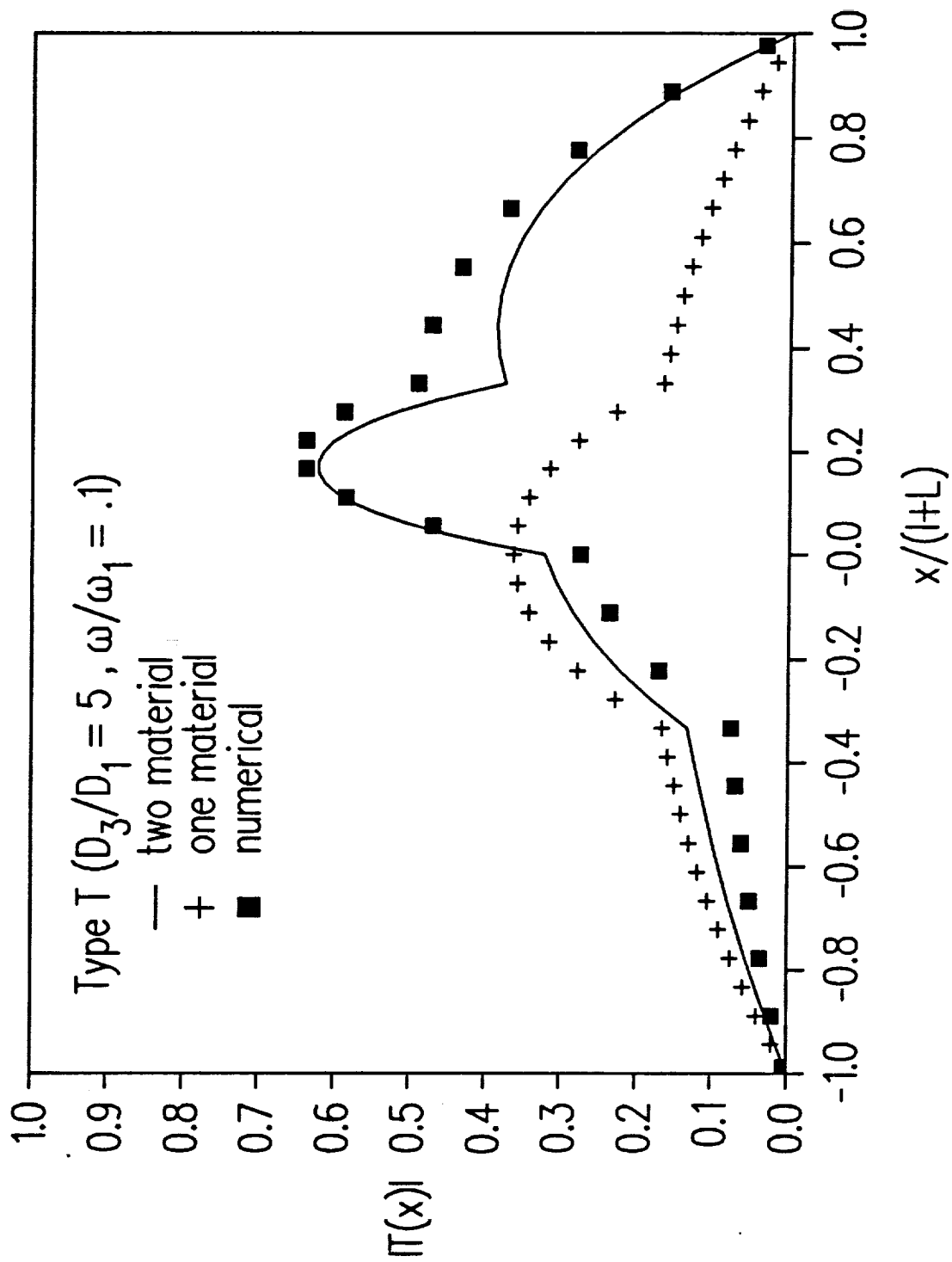
14. Amplitude ratio vs. distance for two material wire. Solid line derived
from Eqs. (36a) and (36b). Crosses are approximate one material solution
Eqs. (14) and (16).

46
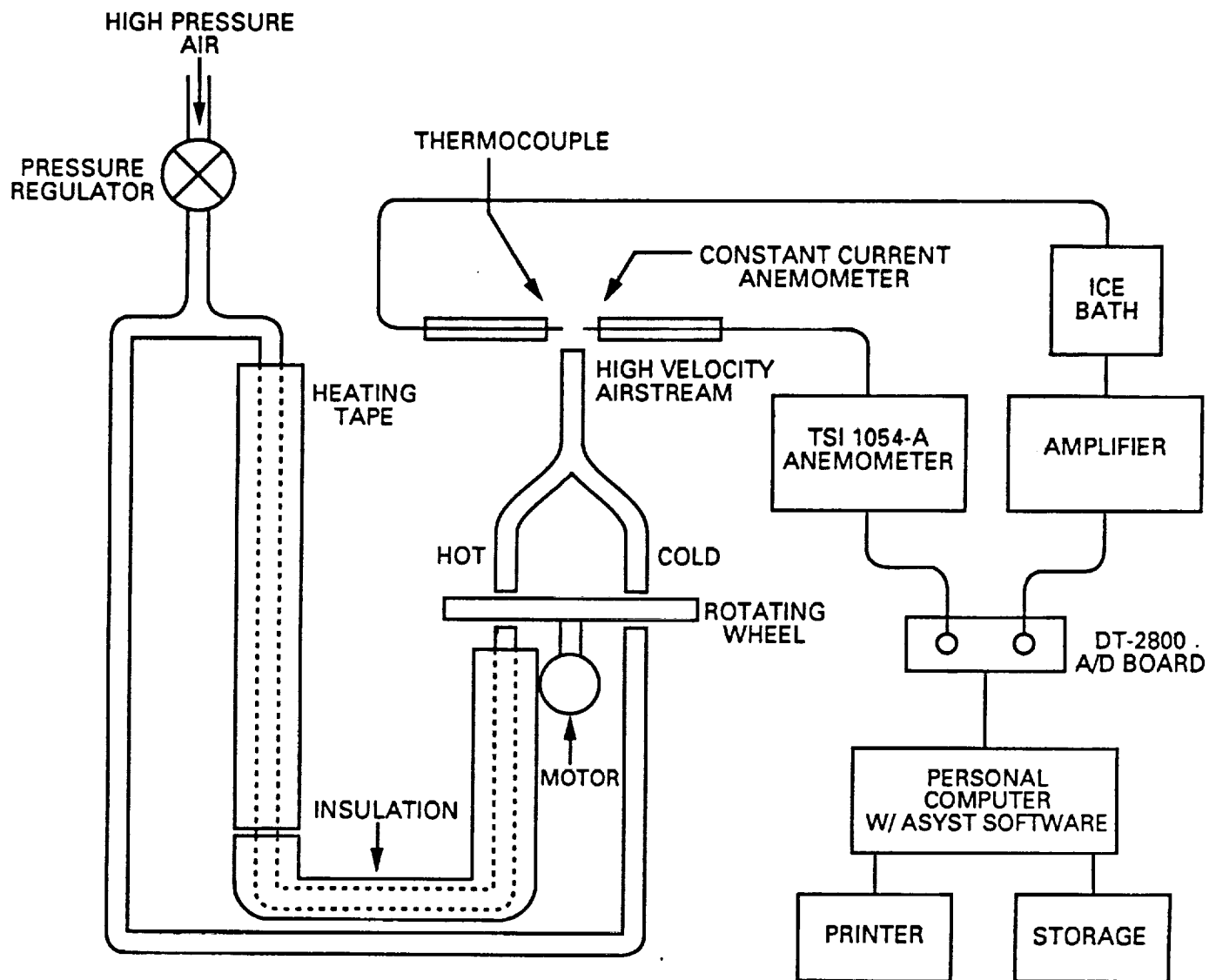
15. Rotating wheel experiment.
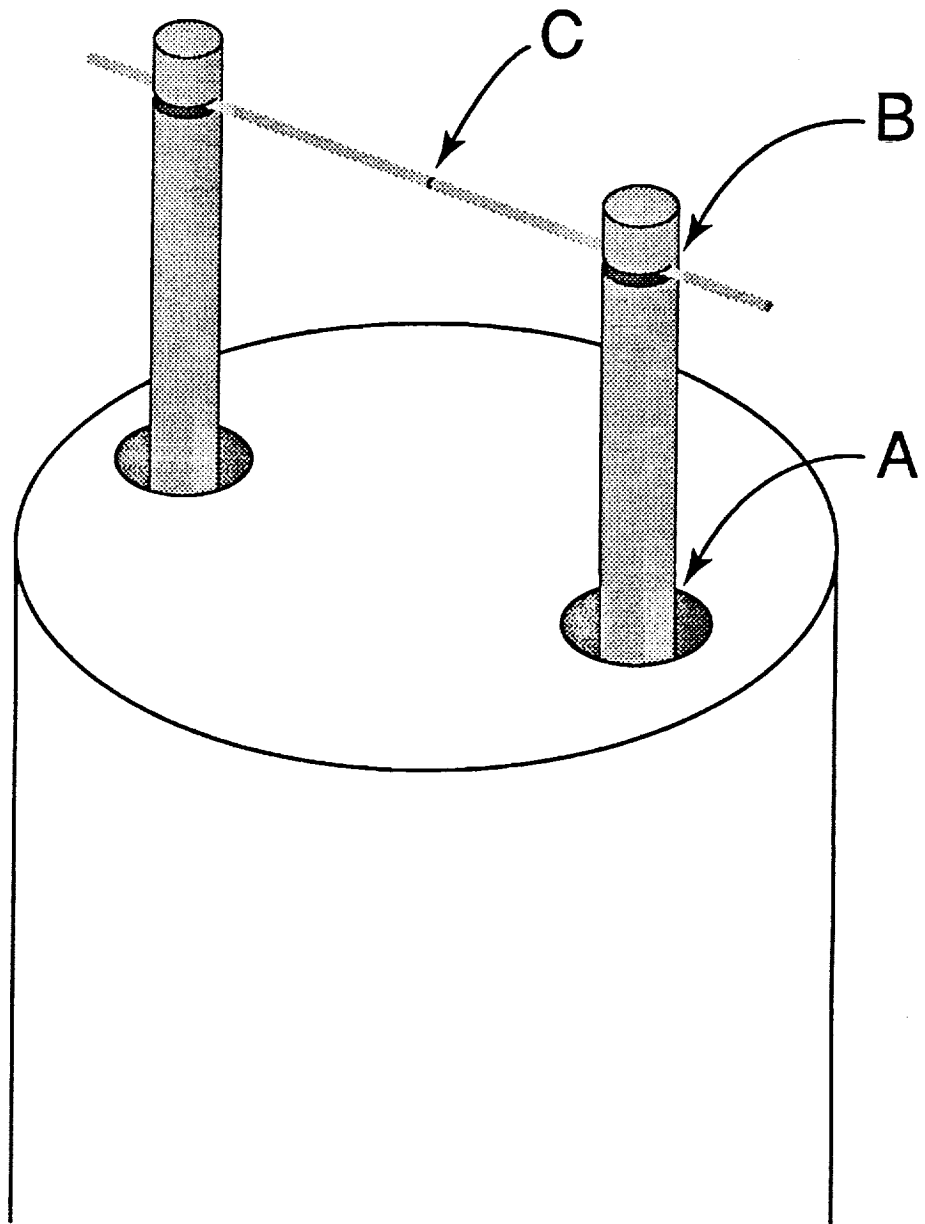
16.   Schematic of test thermocouple

```
FORGET.ALL
REAL DIM[ 1024 ] ARRAY TIME
COMPLEX DIM[ 1024 ] ARRAY TRANS
REAL DIM[ 6 ] ARRAY ANS
REAL DIM[ 1024 ] ARRAY ZMAGO
REAL DIM[ 1024 ] ARRAY ZARGO
INTEGER SCALAR NUM
REAL SCALAR MEN
REAL SCALAR CD
REAL DIM[ 1024 ] ARRAY FREQS
REAL DIM[ 1024 ] ARRAY SIGNAL
INTEGER       dim[ 1024 , 2 ] array DATA.BUFFER


1. CD :=
.0000  DATA.BUFFER :=
LOAD.OVERLAY ACQUIS.SOV
 .0000  1.0000  A/D.TEMPLATE DEMO.TEMPLATE  \ DEFINE AN A/D TEMPLATE
DATA.BUFFER TEMPLATE.BUFFER          \ DECLARE ARRAY AS A TEMPLATE BUFFER
CYCLIC                               \ SET TEMPLATE BUFFER TO CYCLIC MODE
 2048.0000  TEMPLATE.REPEAT          \ SET REPETITIONS FOR I/O INSTRUCTION
 CD  CONVERSION.DELAY                \ CONVERSION RATE (MSECS/SAMPLE)
DEMO.TEMPLATE A/D.INIT               \ INITIALIZE CURRENT A/D TEMPLATE
A/D.IN>ARRAY                         \ A/D INPUT TO TEMPLATES BUFFER
LOAD.OVERLAY WAVEOPS.SOV
1024 REAL RAMP 1 - 2 * CD * 1000 /  TIME :=  \ SET TIME AXIS

DATA.BUFFER  XSECT[ 1 ] 2048 -       \ CHANNEL 1 ON STACK (ANEMOMETER)
SIGNAL := SIGNAL
-2048 / 10 * -55.274 * 353. +        \ CALIBRATE (DEGREES C)
SIGNAL := SIGNAL
0.5 SET.CUTOFF.FREQ                  \ SMOOTH DATA (CYCLES/POINT)
SMOOTH  SIGNAL := SIGNAL
MEAN MEN := SIGNAL
MEN - SIGNAL :=                      \ CENTER ON ORIGIN
TIME SUB[ 1 , 500 , 1 ]  SIGNAL SUB[ 1 , 500 , 1 ]
XY.AUTO.PLOT SIGNAL                  \ PLOT CHANNEL 1
FFT                                  \ TAKE FFT
TRANS := TRANS ZMAG ZMAGO :=         \ MAGNITUDE OF FFT
5 SET.#.POINTS
1 SET.#.OPTIMA
ZMAGO SUB[ 1 , 120 , 1 ] LOCAL.MAXIMA  \ FIND INDEX AND MAX OF MAGNITUDE
SWAP NUM := NUM                      \ INDEX OF MAX MAGNITUDE
1 - CD / 1024. / 1000 * PI *         \ FREQUENCY AT MAX MAGNITUDE
ANS [ 1 ] := ANS [ 1 ] DROP ANS [ 2 ] :=
TRANS [ NUM ] DEG ZARG  ANS [ 3 ] :=    \ ARGUMENT AT MAX MAGNITUDE


DATA.BUFFER XSECT[ 2 ] 2048 -        \ CHANNEL 2 ON STACK (THERMOCOUPLE)
SIGNAL := SIGNAL
.124 * SIGNAL := SIGNAL              \ CALIBRATE (DEGREES F)
0.5 SET.CUTOFF.FREQ                  \ SMOOTH DATA (CYCLES/POINT)
SMOOTH  SIGNAL := SIGNAL
MEAN MEN := SIGNAL
```

```
MEN - SIGNAL :=                          \ CENTER ON ORIGIN
TIME SUB[ 1 , 500 , 1 ]
SIGNAL SUB[ 1 , 500 , 1 ]
XY.DATA.PLOT SIGNAL                      \ PLOT CHANNEL 2
FFT                                      \ TAKE FFT
TRANS := TRANS ZMAG ZMAGO :=             \ MAGNITUDE OF FFT
5 SET.#.POINTS
1 SET.#.OPTIMA
ZMAGO SUB[ 1 , 120 , 1 ] LOCAL.MAXIMA \ FIND INDEX AND MAX OF MAGNITUI
SWAP NUM := NUM                          \ INDEX OF MAX MAGNITUDE
1 - CD / 1024. / 1000 * PI *            \ FREQUENCY AT MAX MAGNITUDE
ANS [ 4 ] := ANS [ 4 ] DROP ANS [ 5 ] :=
TRANS [ NUM ] DEG ZARG ANS [ 6 ] :=      \ ARGUMENT AT MAX MAGNITUDE

CR
." FREQ         MAG         PHI  " CR
ANS [ 1 ] ?  CR
ANS [ 5 ] ANS [ 2 ] /  ? CR
ANS [ 3 ] -1 * ANS [ 6 ] + 180 PI / CD * 1000 / ANS [ 1 ] * - ? CR
FORGET.ALL
```
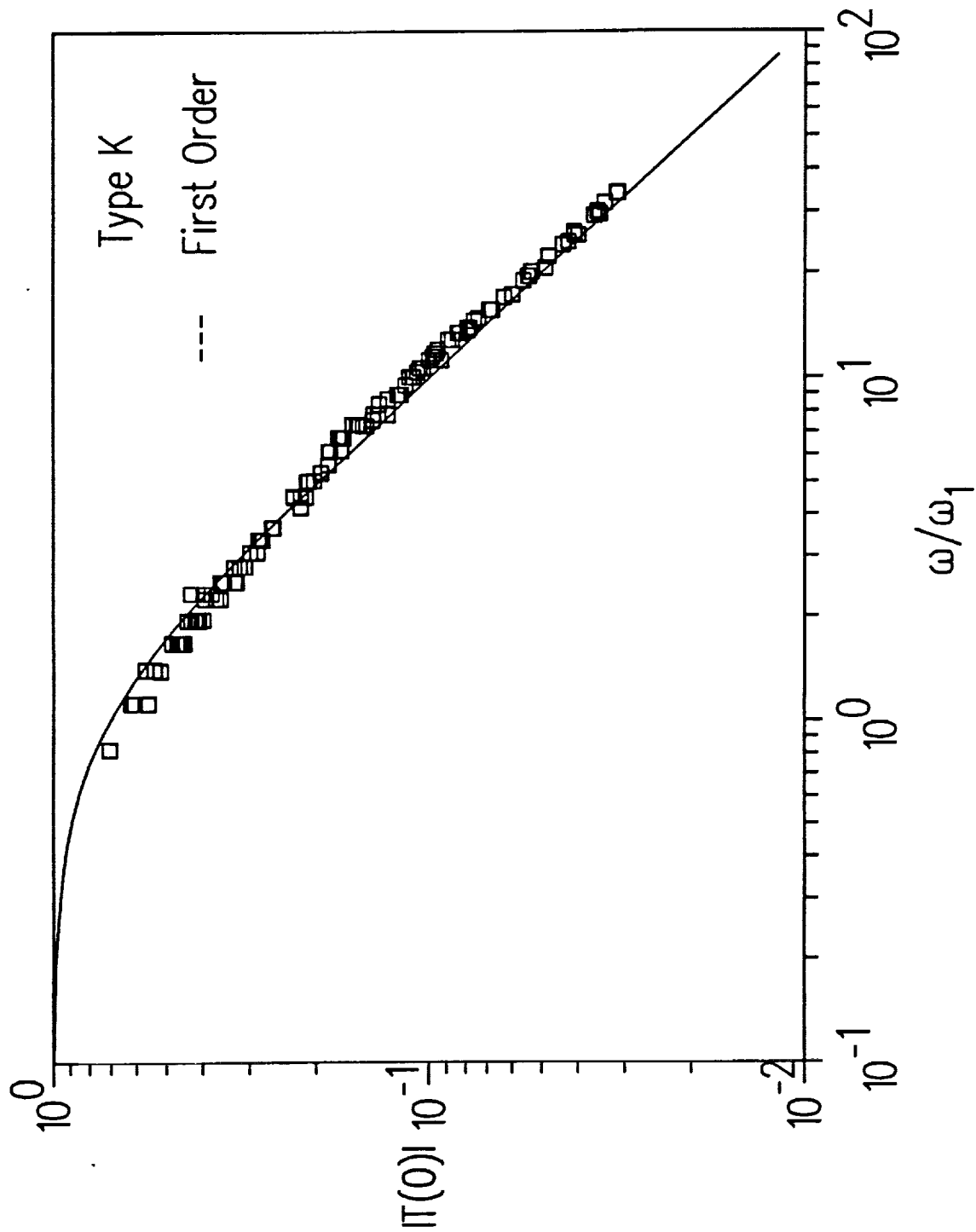
ASYST Version 3.00
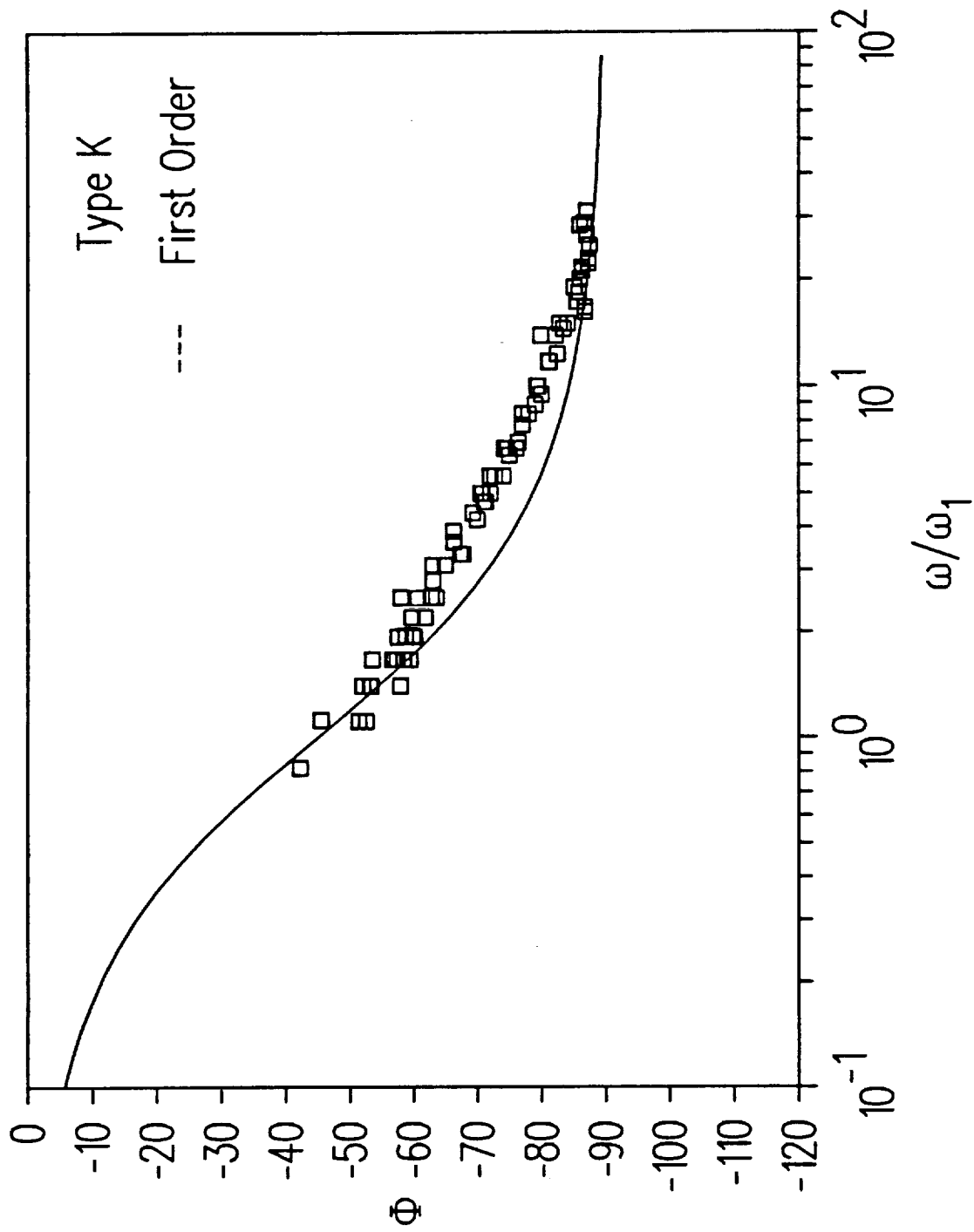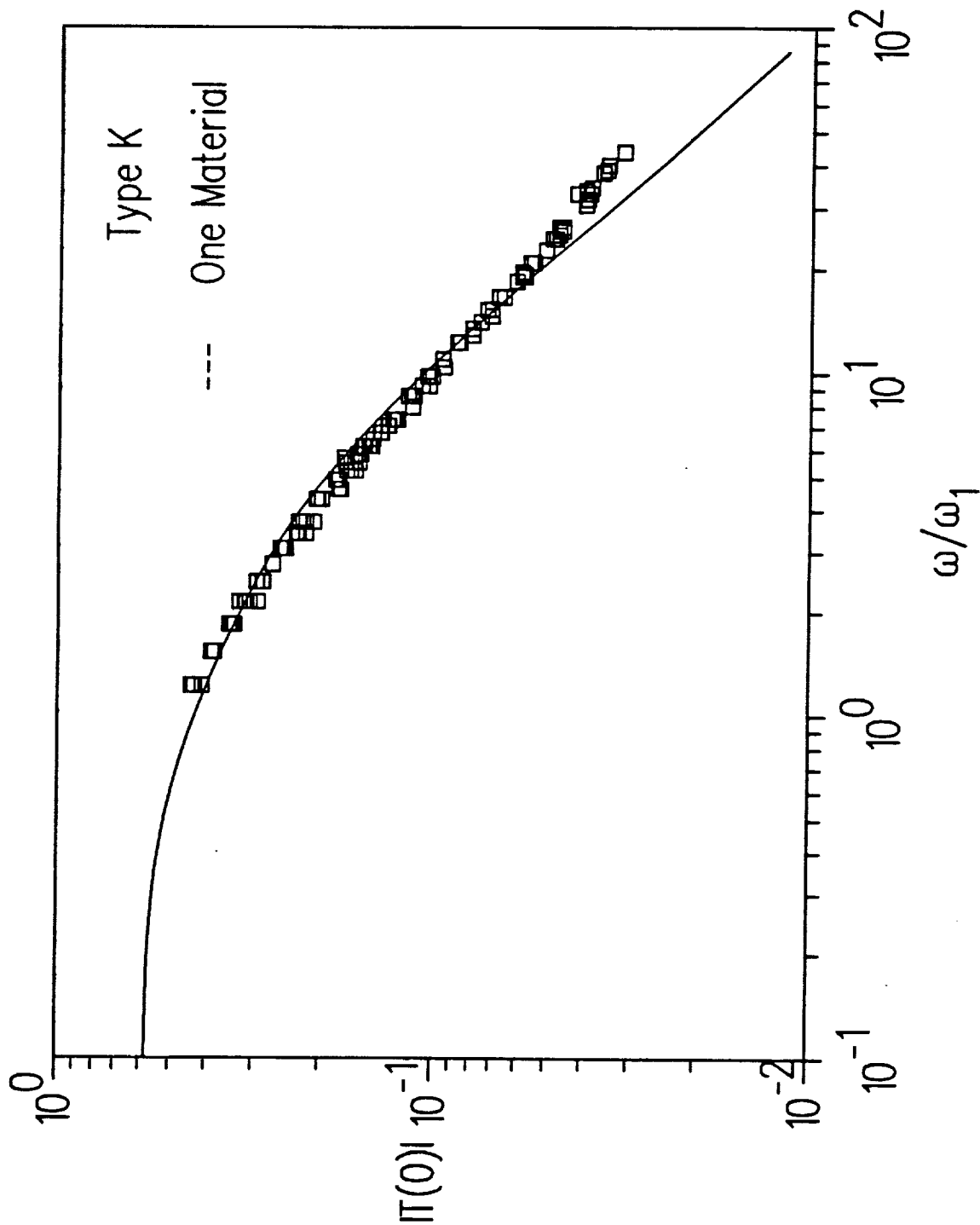Page 2   TEMP3.FOR   03/13/91   11:42:34.65

17. ASYST software
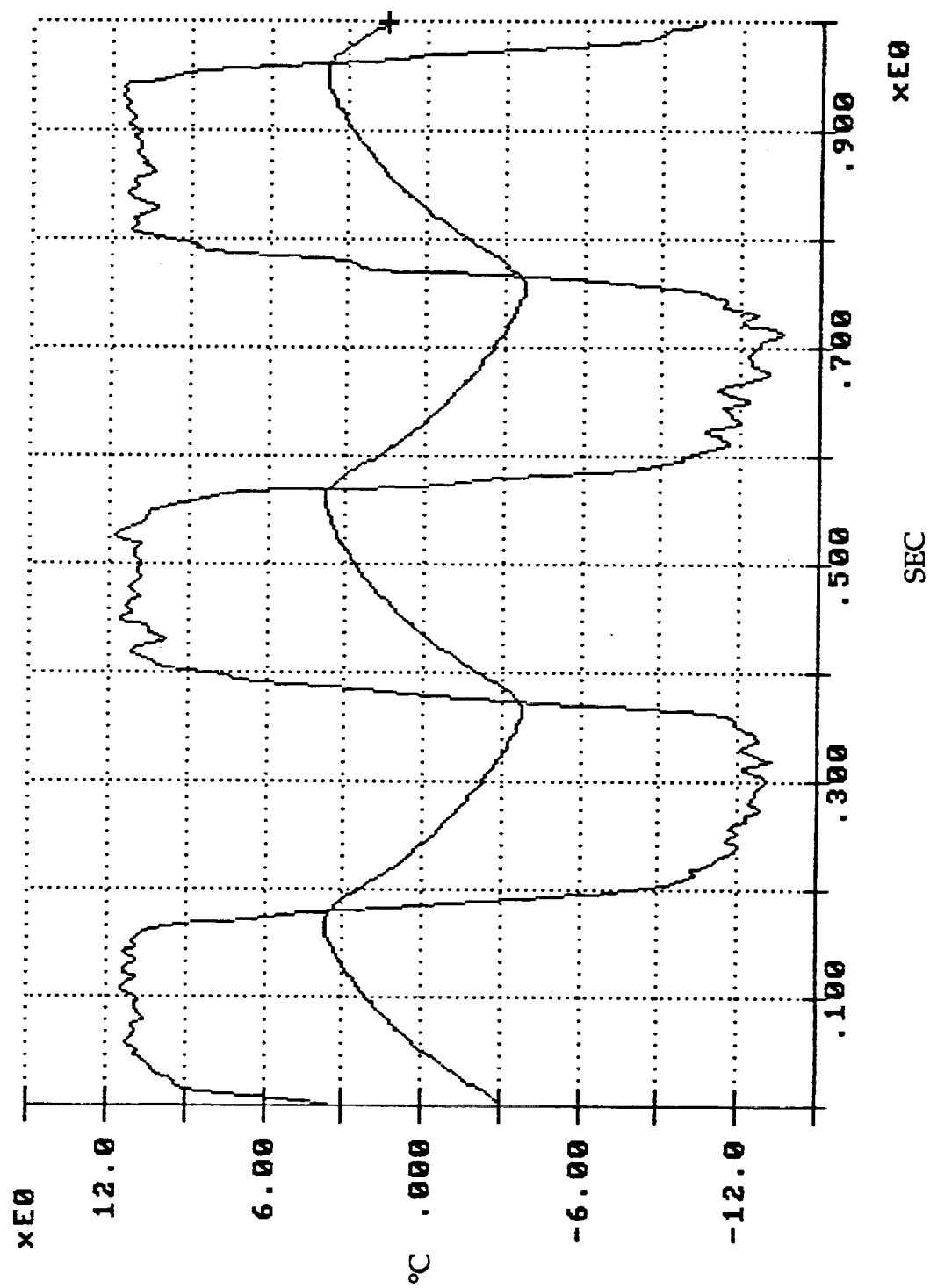
18. Gas temperature profile. Smooth curve is thermocouple response.
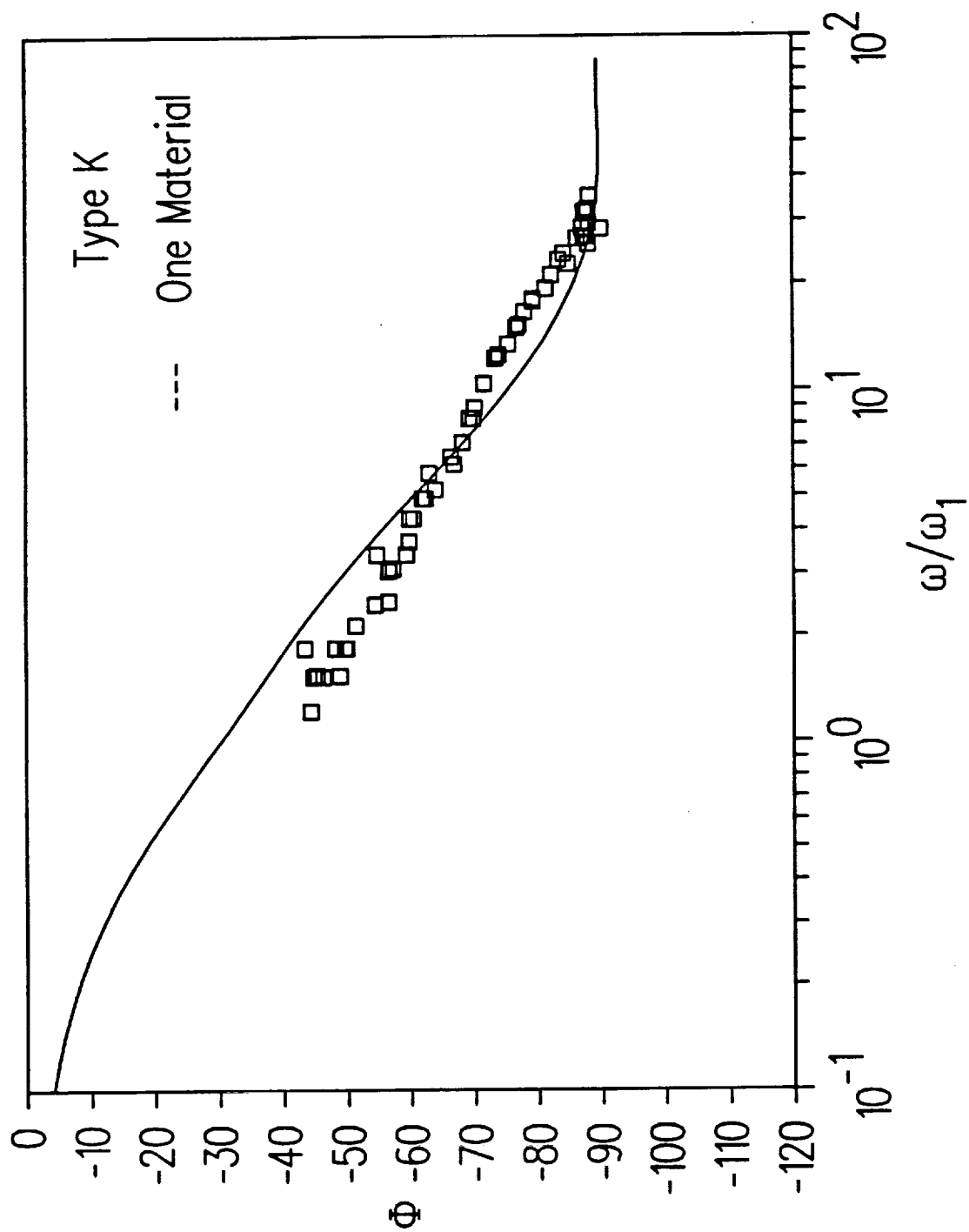
19. Amplitude ratio vs. angular frequency. $\omega_1 = 5.5 \text{ sec}^{-1}$, $\alpha = .059 \text{ cm}^2 / \text{sec}$.

20. Phase angle vs. angular frequency. $\omega_1 = 5.5\ sec^{-1}$, $\alpha = .059\ cm^2/sec$.

53

21. Amplitude ratio vs. angular frequency. Solid line is Eq. (32).

ω = 5 0 sec⁻¹ (ν = 050 cm² / sec

54

22. Phase angle vs. angular frequency. Solid line is derived from Eq. (32). $\omega_1 = 5.0 \ sec^{-1}$, $\alpha = .059 \ cm^2/sec$.